



## Novel state estimation framework for humanoid robot

Hyoin Bae, Jun-Ho Oh \*

Mechanical Engineering, Korea Advanced Institute of Science and Technology (KAIST), 291 Daehak-ro, Yuseong-gu, Daejeon 34141, Republic of Korea

### HIGHLIGHTS

- The proposed estimator framework consists of two estimator loops.
- One loop for the state estimation and the other loop for the disturbance estimation.
- The disturbance estimated in the disturbance estimation loop is provided as feedback.
- The correlation between state and disturbance is calculated automatically.
- The proposed estimator complements the fundamental limitations of the original KF.

### ARTICLE INFO

#### Article history:

Received 14 December 2016  
Received in revised form 28 June 2017  
Accepted 27 September 2017  
Available online 12 October 2017

#### Keywords:

Humanoid state estimation  
Robust Kalman filtering  
Modeling error compensation  
Humanoid robot

### ABSTRACT

This study proposes a new Kalman filter-based framework for humanoid robot state estimation. The conventional Kalman filter generates optimal estimation solutions only when the nominal equations of the model and measurement include zero-mean, uncorrelated, white Gaussian noise. Because a humanoid robot is a complex system with multiple degrees of freedom, its mathematical model is limited in terms of expressing the system accurately, resulting in the generation of non-zero-mean, non-Gaussian, correlated modeling errors. Therefore, it is difficult to obtain accurate state estimates if the conventional Kalman filter-based approaches are used with such inexact humanoid models. The proposed modified Kalman filter framework consists of two loops: a loop to estimate the state, and a loop to estimate the disturbance generated by the modeling errors (a dual-loop Kalman filter). The disturbance values estimated by the disturbance estimation loop are provided as feedback to the state estimation loop, thereby improving the accuracy of the model-based prediction process. By considering the correlation between the state and disturbance in the estimation process, the disturbance can be accurately estimated. Therefore, the proposed estimator allows the use of a simple model, even if it implies the presence of a large modeling error. In addition, it can estimate the humanoid state more accurately than the conventional Kalman filter. Furthermore, the proposed filter has a simpler structure than the existing robust Kalman filters, which require the solution of complex Riccati equations; hence, it can facilitate recursive online implementation. The performance and characteristics of the proposed filter are verified by comparison with other existing linear/nonlinear estimators using simple examples and simulations. Furthermore, the feasibility of the proposed filter is verified by implementing it on a real humanoid robot platform.

© 2017 Elsevier B.V. All rights reserved.

### 1. Introduction

In recent years, humanoid robots with a variety of types and purposes have been introduced. A humanoid robot is a multi-joint robot whose shape is similar to that of a human. It has two legs for mobility, and two arms for manipulation. Among the various types of robots, it is regarded as the most appropriate robot for collaborating with humans, because its operating environment and the available tools are already suited for human activities. Owing to these advantages, a number of research institutes have

developed humanoid robots with various modes and structures. Some representative humanoid robots are HUBO, Atlas, Asimo, HRP, and Schaft [1–5].

Previously, such robots were only required to operate in limited environments. However, they are now required to take on various missions in diverse environments. For example, the robots are now required to not only assist people in home or office environments, but also perform dangerous or difficult tasks that cannot be performed by humans, in disaster scenarios or outdoor environments. Toward this end, robot hardware and control algorithms should be developed harmoniously. One of the key requirements is a technology for estimating the robot's state (center-of-mass kinematics, robot's attitude, contact status, etc.) rapidly and accurately.

\* Corresponding author.

E-mail addresses: [pos97110@kaist.ac.kr](mailto:pos97110@kaist.ac.kr) (H. Bae), [jhoh8@kaist.ac.kr](mailto:jhoh8@kaist.ac.kr) (J.-H. Oh).

An accurate robot state estimation facilitates the use of greater sophistication in the design of feedback controllers. Furthermore, it allows increasing the controller gain so that the humanoid robots can respond to dynamic environments more effectively. Accordingly, many humanoid robots employ their own state estimators. A large number of these estimators are based on the Kalman filter [6–19]. When the model and measurement noises are zero-mean, uncorrelated, and white, the Kalman filter (KF) is an optimal linear filter, which can minimize the error covariance based on both the system model and the collected measurements [20–22].

Many studies have proposed humanoid state estimator frameworks based on KFs. The most basic studies have configured the KF using the linear inverted pendulum model (LIPM), which has been widely used in humanoid robot control [6–8]. The LIPM is an extremely simplified model, in which humanoid movements are represented as a point mass with a constant center of mass (COM) height [23,24]. In [6], a KF was configured using an LIPM based on the measured zero moment point (ZMP) to estimate the kinematics of the robot's COM. In [7], a KF was configured by combining a discretized LIPM and forward kinematic information in order to improve the above-mentioned KF. In [8], a KF was configured by incorporating the COM and foot positions into the state vector, using the walking phase information, and establishing a number of constraints as measurements. In [9], a force and acceleration correlation equation was employed as the KF process model, and the forward kinematic information and moment equilibrium equations were used as measurement factors in order to estimate the COM's position and velocity. In [10], the base and joint velocities were estimated using a steady-state KF (SSKF) after decoupling the full-body dynamics into base kinematics and joint kinematics. Here, the forward kinematic information was used as measurement data and the force/torque (F/T) sensor data was used to adaptively modify the measurement matrix. Similarly, in [11,12], inertial measurement unit (IMU) information was added to the model input, and 3D-map information obtained through LiDAR was added as measurement data to construct a KF that estimated the robot kinematics. Further, a study was conducted to configure a KF for quadruped robot state estimation by incorporating base kinematics, foot pose, and gyro bias into the state vector [13]. Here, IMU information was used as the model input, and the forward kinematic information was used as measurement data. The above-mentioned study was extended to the case of humanoid robots [14]; information about the rotation limitation of the sole was added to the state and measurement. In [15], a KF was used to estimate a hexapod robot's base kinematics. The angular acceleration was estimated with a multi-accelerometer, and the estimation model was modified according to the stance phase and flight phase. Furthermore, studies have been conducted to estimate the six-degrees-of-freedom (6-DOF) dynamic deformation of the foot's flexible part – which is considered as a characteristic of most humanoid robots – using a KF [16,17]; the IMU information was used as measurement data, and additional contact information was used as constraints in the filter. In [18], the data of a gyro sensor attached to the lower body link for estimating the joint velocity of a hydraulic drive humanoid was used as additional Kalman filter measurement data. In [19], the linear velocity, angular velocity, and foot wrench were estimated using the rigid body dynamics of the foot.

Some studies have investigated other estimation methods besides state estimation using a KF [25–28]. For a KF or moving horizon estimator, the model should be expressed in state space form during filter design. To overcome this drawback, a study has investigated estimator design based on quadratic programming, by minimizing an  $\|Ax - b\|^2$ -type cost function while satisfying the various inequality constraints of humanoid robots [25]. In this study, the base kinematics and joint torque were used as

state information. Another study has investigated estimator design using a complementary filter [26]. The complementary filter was configured by using the complementary frequency properties of the double-integral-of-acceleration (DIA)-based position and the COM position obtained through model-based forward kinematics. Further, the cut-off frequency was set according to the force/torque (F/T) sensor measurement. In [27], a  $H_2$  optimal filter was designed to estimate the humanoid state; this filter minimizes the effect of the input disturbances and measurement noise, in order to overcome the problem of KF configuration by inaccurate models.

As such, a number of studies have used KFs for state estimation (i.e., COM kinematics and contact status), of humanoid robots. The KF is widely used not only because of its optimality characteristics but also because it allows a convenient implementation of physical systems expressible in a recursive discrete form. The elements that do not belong to the basic model (e.g., modeling error and input disturbance) are generally considered to be model noise (or model disturbance); the KF guarantees optimality when both the model noise and the measurement noise are zero-mean, white, uncorrelated, and Gaussian distributed. Even when these noises are not Gaussian distributed, the KF is the best linear state estimator for minimum variance estimation [22]. However, there is a fundamental limitation on the optimality of the KF. If the model and measurement noises are non-zero-mean, non-white, or correlated, the conventional KF does not guarantee optimal state estimates.

It is impossible for humanoid robots to perform accurate modeling without physical errors because they are complex multi-body/multi-joint systems. Therefore, when using conventional KFs, the inaccuracy of the obtained estimation results is proportional to the modeling errors and disturbances. As a result, a considerable number of the above-mentioned studies using conventional KFs and curbing humanoid robots by fitting them with simple system models inevitably suffer from fundamental limitations.

A few studies have analyzed (and attempted to address) the limitations of KFs in humanoid state estimation. In [29], the effect of modeling errors and unknown forces on the estimation results was analyzed in the case of state estimation using a KF. In [30], a KF was configured on the basis of an LIPM model – as in [6] – in order to estimate the COM kinematics; the problem was solved by considering the LIPM modeling error as a “COM offset” term that could be estimated. In contrast, another study solved the problem of modeling errors and disturbances by using an LIPM as the system model and adding an extra term to the system input [31]; the difference between the desired and measured torques was considered to be the result of unknown errors, and was then modeled as an extra term. This study was extended to nonlinear ZMP model at [32]. The nonlinear ZMP model facilitated the 3-D COM position estimation and increased the estimation accuracy. In [33], the problem was solved by augmenting the KF estimation error into the state vector when there was uncertainty in the model matrix  $A$  and in the measurement matrix  $H$ . However, this approach is limited to cases in which the model uncertainties are bounded and coupled. The alternatives proposed in the above-mentioned studies basically modify the system model or state vector only slightly and employ the conventional KF without fundamental changes; therefore, they cannot overcome the drawbacks of the conventional KF. Furthermore, the above-mentioned approaches are only applicable to specific state parameters or specific models; hence, they cannot be generalized or easily applied to systems that are modeled differently.

Therefore, it is necessary to develop a humanoid state estimator framework that is robust to modeling errors or disturbances while using simple models and can overcome the limitations of the existing approaches. The present study proposes a novel KF framework for humanoid robot state estimation. The proposed

modified KF consists of two loops: one KF loop to estimate the state, and a second KF loop to estimate the disturbance resulting from the modeling errors (dual-loop Kalman filter). The disturbance value estimated in the disturbance estimation loop is provided as feedback to the state estimation loop, and is thus reflected in the state estimation process. With this disturbance compensation, the state estimation accuracy ultimately increases. Consequently, this disturbance compensation acts like a residual-error-integration compensator. To enhance the disturbance estimation accuracy, the correlation between the state and the disturbance is elaborately considered during the estimation process. The new state estimator can provide more accurate estimates than the original KF, even though using simple models with non-zero mean, correlated, and non-Gaussian errors. Additionally, it has a simpler structure than the existing robust KFs, which require the solution of complex Riccati equations and pre-defined uncertainty boundary conditions. These advantages will be demonstrated through simple examples, simulations, and frequency characteristic analysis.

The remainder of this paper is organized as follows. Section 2 briefly reviews the structure, characteristics, and limitations of the conventional KF. Section 3 describes the concept and structure of the proposed novel estimator, and presents simple examples of its use. Section 4 compares the humanoid state estimation results obtained with the proposed estimator with those of existing methods. Finally, Section 5 concludes the paper and briefly explores some directions for future work.

## 2. Basic knowledge about conventional Kalman filter

This section briefly reviews the basic structure, characteristics, and limitations of the KF—which is widely used for estimation in various fields, including humanoid robot state estimation.

### 2.1. Kalman filter structure

The Kalman filter (KF) is a linear quadratic estimator; it minimizes the covariance of the estimation error via both modeling and measurement of the target system [20–22]. The KF was originally proposed by Kalman in 1961. Since then, many variants of the KF have been introduced, such as the extended Kalman filter (EKF) [34], unscented Kalman filter (UKF) [35], and ensemble Kalman filter (EnKF) [36]; these variants are also partially applicable to nonlinear systems. The KF is characterized by a simple structural property, a recursive nature, and convenience of implementation in discrete form. Owing to these advantages, the KF has numerous applications in various fields such as aviation, meteorology, signal processing, and robotics. As discussed in Section 1, the KF is also used for humanoid robot state estimation. The basic concepts and structure of the KF are described below.

Let us assume that a real physical system is represented in discrete form as follows (in this paper, subscript  $k$  denotes the discrete time step index).

$$x_k = f(x_{k-1}, u_{k-1}) = A_{k-1}x_{k-1} + B_{k-1}u_{k-1} + w_{k-1} \quad (1)$$

$$y_k = h(x_k) = H_kx_k + v_k \quad (2)$$

where  $x_k \in R_n$  is the system's state vector,  $u_k \in R_p$  is the system's known control input vector,  $y_k \in R_m$  is the measurement vector,  $A_k \in R_{n \times n}$  is the state transition matrix (process matrix),  $B_k \in R_{n \times p}$  is the input transition matrix, and  $H_k \in R_{m \times n}$  is the measurement matrix. Further,  $w_k \in R_n$  is the (un-modeled) process disturbance vector and  $v_k \in R_m$  is the measurement noise vector.

The original KF works in two steps: time update (prediction step), which predicts the next state based on the previous state and the system dynamics model, and measurement update (correction step), which creates a final state estimate after

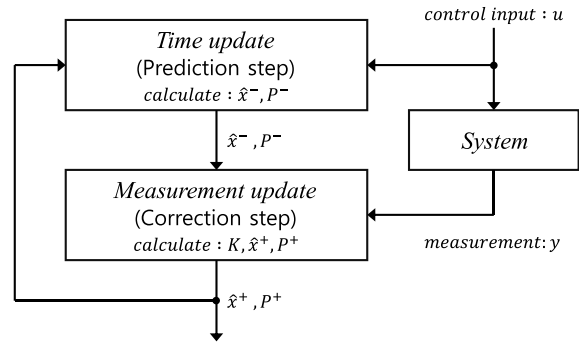


**Fig. 1.** Basic structure of conventional (original) Kalman filter. It works in two steps: time update and measurement update. Discrete time step index subscript  $k$  is omitted for simplicity.

correcting the predicted state on the basis of the current measurement (Fig. 1). The steps are expressed by the following equations.

- Time update (prediction step)

$$\hat{x}_k^- = A_{k-1}\hat{x}_{k-1}^+ + B_{k-1}u_{k-1} \quad (3)$$

$$P_k^- = A_{k-1}P_{k-1}^+A_{k-1}^T + Q_k \quad (4)$$

- Measurement update (correction step)

$$K_k = P_k^- H_k^T (H_k P_k^- H_k^T + R_k)^{-1} \quad (5)$$

$$\hat{x}_k^+ = \hat{x}_k^- + K_k(y_k - H_k\hat{x}_k^-) \quad (6)$$

$$P_k^+ = (I - K_k H_k) P_k^- \quad (7)$$

where the hat denotes estimated values,  $\hat{x}_k^- \in R_n$  is the a priori state estimate – the predicted state before the measurement update process – and  $\hat{x}_k^+ \in R_n$  is the a posteriori state estimate—the final estimated value after the measurement update process. Further,  $P_k^- \in R_{n \times n}$  and  $P_k^+ \in R_{n \times n}$  denote the a priori and a posteriori estimate error covariance matrices, respectively, which are defined as follows:

$$P_k^- = E[e_k^- e_k^{+T}] = E[(x_k - \hat{x}_k^-)(x_k - \hat{x}_k^-)^T] \quad (8)$$

$$P_k^+ = E[e_k^+ e_k^{+T}] = E[(x_k - \hat{x}_k^+)(x_k - \hat{x}_k^+)^T] \quad (9)$$

where  $E[\cdot]$  stands for the stochastic expectation operator for RV (random variables);  $K_k$  is the Kalman gain, which determines the reliability weight between the model-based prediction and the measurement;  $Q_k = E[w_k w_k^T] \in R_{n \times n}$  and  $R_k = E[v_k v_k^T] \in R_{m \times m}$  denote the process noise and measurement noise covariance matrices, respectively. According to Eq. (5), the larger the value of  $Q_k$  (i.e., the larger the model process noise/disturbance), the larger the Kalman gain. On the other hand, the larger the value of  $R_k$ , the smaller the Kalman gain.

### 2.2. Limitations of the Kalman filter

The KF can produce optimal estimates in the sense of minimizing the error covariance, but its optimality is limited to cases in which the modeling noise (disturbance  $w_k$ ) and measurement noise ( $v_k$ ) are zero mean, white, and Gaussian (normal) distributed. In other words, the optimality of the KF is satisfied only when

$w_k$  and  $v_k$  in Eqs. (1) and (2) are white, independent, and satisfy  $p(w_k) \sim N(0, Q_k)$  and  $p(v_k) \sim N(0, R_k)$ . Here,  $p(\cdot)$  denotes the probability density function, and  $N(\bar{m}, \sigma^2)$  denotes a Gaussian distribution RV (random variables) with mean  $\bar{m}$  and variance  $\sigma^2$ . Of course, it is still the best linear state estimator even if the noises are not Gaussian, but its optimality will be limited if those noises have non-zero-mean, are non-white, or are correlated [21,22].

Let  $A_{real}$  be the accurate model matrix of a real system. This is certainly an unknown element. In addition, let  $A_{model}$  be the matrix that models the system for state estimation or control. Assuming that the difference (modeling error) between the two matrices is  $\Delta A$ , the relation between them can be expressed as follows:

$$A_{real} = A_{model} + \Delta A \quad (10)$$

In addition, let us assume that an unknown effect  $d_k \in R_p$  is applied to the system control input. The state transition of the real system can then be expressed as follows:

$$\begin{aligned} x_k &= A_{real,k-1}x_{k-1} + B_{k-1}(u_{k-1} + d_{k-1}) \\ &= (A_{model,k-1} + \Delta A_{k-1})x_{k-1} + B_{k-1}(u_{k-1} + d_{k-1}) \\ &= A_{model,k-1}x_{k-1} + B_{k-1}u_{k-1} + \underbrace{\Delta A_{k-1}x_{k-1} + B_{k-1}d_{k-1}}_{w_{k-1} (=disturbance)} \end{aligned} \quad (11)$$

Comparing Eqs. (1) and (11), the sum of the errors (the disturbance) resulting from the modeling error and the control input noise can be expressed as follows:

$$w_k \triangleq \Delta A_k x_k + B_k d_k \quad (12)$$

As such, if there is a large difference between the model and the real system, it would be difficult for the disturbance  $w_k$  to be zero-mean and Gaussian distributed ( $p(w_k) \not\equiv N(0, Q_k)$ ). In addition, this disturbance would be correlated, and therefore non-white. In this case, it would be difficult to find an optimal estimated value using conventional KFs. Note that, as shown in Eq. (12), the total disturbance  $w_k$  is correlated with the state  $x_k$ . This characteristic is important and will be discussed later for the case of the new estimator induction process.

For simple systems, a system model  $A_{model}$  can be modeled to closely match the real system. However, for multi-joint/multi-body humanoid robots, it is nearly impossible to precisely reflect the physical characteristics of the real system in the model  $A_{model}$ , owing to the existence of various unknown elements and to system complexity. For example, although many humanoid robots employ an LIPM in the control and estimation process owing to its simplicity and efficiency, the LIPM – which is characterized by a single mass and a constant height – is too simple for expressing the physical characteristics of humanoid robots, which are multi-body dynamic systems; therefore, it is unreasonable to consider the un-modeled elements as constituting zero-mean, uncorrelated (white) noise. Consequently, a number of approaches that use conventional KFs as a state estimation framework and adopt simple system models are basically vulnerable to non-zero mean and non-Gaussian modeling errors (disturbances).

If a system model is configured using a highly complex mathematical approach (i.e., full-body dynamics or a centroidal model), it can produce more accurate estimates than those using a simple approach (because  $w_k$  will better approximate white Gaussian noise). However, this will require excessively high computation power during the estimation and control processes, and the  $Q_k$  and  $R_k$  matrix tuning processes could become very complicated during the KF implementation step. Therefore, a complex mathematical approach is not the preferred option for systems requiring fast estimation response with limited computing power (as is the case of humanoid robots).

Therefore, there is a need for a robust estimator capable of mitigating the problem of increasing estimation error caused by

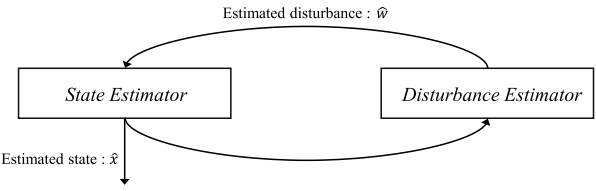


**Fig. 2.** Basic concept of proposed estimator framework. Discrete time step index  $k$  is omitted for simplicity.

unknown modeling errors (rather than by zero-mean white noise) while using limited computing power. The next section describes the proposed dual-loop Kalman filter, which is a robust solution to this problem.

### 3. Dual loop Kalman filter

This section introduces the basic concept, structure, and equations of the proposed estimator framework, which is named the dual-loop Kalman filter (DLKF). In addition, the proposed DLKF is compared with the conventional KF using simple examples and frequency response analysis.

#### 3.1. Concept of the proposed Kalman filter

The simplified structure of the proposed DLKF is shown in Fig. 2. The state estimator (left block) estimates the system state that needs to be known, as with the conventional KF. The disturbance estimator (right block) estimates the disturbance  $w_k$  generated by un-modeled elements in the state estimator (such as conventional disturbance observer). Let us assume that the disturbance estimated by the disturbance estimator is  $\hat{w}_k \in R_n$ . The estimated disturbance is fed back to the state estimator and then used when calculating the a priori state estimate  $\hat{x}_k^-$  in the prediction step (model-based forecast) of the KF, as it is combined with the model equation. The model-based prediction step of the original KF (given by Eq. (3)) is therefore modified as follows:

$$\hat{x}_k^- = \underbrace{A_{k-1}\hat{x}_{k-1}^+ + B_{k-1}u_{k-1}}_{\text{original model based prediction}} + \underbrace{\hat{w}_{k-1}}_{\text{disturbance compensation}} \quad (13)$$

If the disturbance estimator can estimate  $\hat{w}_k$  such that it is close to the real  $w_k$  given by Eq. (12), a relatively robust and accurate a priori state estimate (forecast) can be obtained using Eq. (13), even if a modeling error is present. The accuracy of the final state estimation result after the measurement update step will thus ultimately increase.

Some studies have attempted to overcome the problems caused by un-modeled elements in the filter step. In [37], a modified Luenberg observer was proposed, which makes the estimation errors generated by modeling errors approach zero by using Lyapunov's stability criteria. In [38], a finite horizon Kalman filter was designed, which is robust to deterministic additive noise and stochastic multiplicative noise existing in the model. Both above-mentioned studies guarantee an upper bound on the state estimation error variance. However, they both not only require norm-bounding information about the modeling error (uncertainty) to be known in advance, but also require high-dimensional Riccati equations to be solved online for a time-varying system. Therefore, they cannot be used for humanoid robots.

In [39–41], a disturbance observer was designed for manipulation (or motion control) by setting the difference between the estimated (expected) torque obtained from the dynamics equation and the actual torque to the disturbance measurement value (equivalent disturbance). Although these approaches are disadvantageous

(because the observer is limited by the torque disturbance), they propose an interesting and useful concept for the disturbance observer. Another study transformed the disturbance observing problem into a tracking problem [42]. Here, the difference between the a priori estimate  $\hat{x}^-$  and the a posteriori estimate  $\hat{x}^+$  in the KF was attributed to the disturbance; the observing problem for following the disturbance was then transformed into a tracking problem. The sliding-mode control-based tracking problem was configured by setting the difference between the two estimates (error and disturbance) as the control input. In [43–45], the observed disturbance was reflected in the conventional Luenberg observer, which can be regarded as a basic version of a KF. The difference between the final estimated state and the model-predicted value at the previous step was assumed to be the disturbance at the current step. For noisy disturbance, a Q-filter ( $\hat{w}_k = Q_{\text{filter}} \cdot (\hat{x}_k - f(\hat{x}_{k-1}, u_{k-1}))$ ) was adopted. The frequency characteristics of this estimator and the effects of the Q-filter design were analyzed. In another study, this concept was extended to the KF [46].

The new KF framework proposed in the present study is influenced by the above-mentioned studies. The estimator proposed here exploits the advantages of the above-mentioned approaches in the maximum possible extent, and is designed for convenient and practical implementation. Moreover, it performs state estimation more easily and intuitively than the previous methods. In particular, it is designed to be used without the requirements for particular information – such as the model of the disturbance or bounds on the model uncertainty – that characterize previous studies.

Specifically, the present study employs dual KFs. As shown in Fig. 2, the new estimator consists of two KF loops: one is used for state estimation (on the left side of Fig. 2), and the other for disturbance estimation (on the right side). The newly proposed estimator framework is called a dual-loop Kalman filter (DLKF). The estimated a posteriori disturbance obtained from the disturbance-estimating KF is fed back to the prediction step of the state-estimating KF and then used to calculate the a priori state estimate. Assuming that the a priori and a posteriori disturbance estimates calculated in the disturbance-estimating KF loop are expressed as  $\hat{w}_k^- \in R_n$  and  $\hat{w}_k^+ \in R_n$ , respectively, Eq. (13) is therefore modified as follows:

$$\hat{x}_k^- = A_{k-1}\hat{x}_{k-1}^+ + B_{k-1}u_{k-1} + \hat{w}_k^- \quad (14)$$

It is now necessary to define which value can be considered to be the disturbance measurement ( $y_w \in R_n$ ) required for the disturbance-estimating KF. In the present study, the current step disturbance measurement is assumed to be the difference between the “a posteriori state estimate” and the “model-based calculation part of the a priori state estimate” calculated from the previous step by the state-estimating KF. Therefore, the proposing disturbance estimation KF can be considered to be a kind of time-delayed disturbance observer (the disturbance estimate for the current step is calculated from the previous step information: one step delayed). In other words, from the viewpoint of the original KF, the difference between  $\hat{x}^+$  and  $\hat{x}^-$  is considered as the effect of disturbance. This can be expressed by the following equation.

$$y_{w,k} = \hat{x}_k^+ - \underbrace{f(\hat{x}_{k-1}^+, u_{k-1})}_{\text{in original K.F.}} = \hat{x}_k^+ - A_{k-1}\hat{x}_{k-1}^+ - B_{k-1}u_{k-1} \quad (15)$$

In order to determine whether this equation is appropriate and based on a solid assumption, it can be expanded using the basic KF filter equation and probabilistic concept as follows:

$$\begin{aligned} E[y_{w,k}] &= E[\hat{x}_k^+ - f(\hat{x}_{k-1}^+, u_{k-1})] \\ &= E[\hat{x}_k^- + K_k(y_k - H_k\hat{x}_k^-) - f(\hat{x}_{k-1}^+, u_{k-1})] \quad (\text{from Eq. 6}) \end{aligned}$$

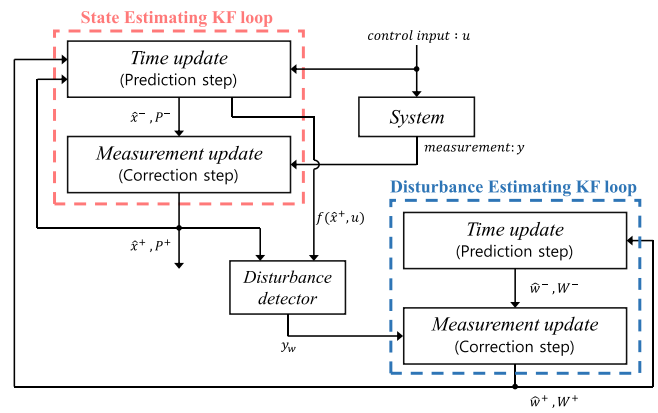


**Fig. 3.** Proposed dual-loop Kalman filter (DLKF). It consists of two KF loops: one for state estimation and one for disturbance estimation. Discrete time step index  $k$  is omitted for simplicity.

$$\begin{aligned} &= E[f(\hat{x}_{k-1}^+, u_{k-1}) + \hat{w}_{k-1} + K_k(H_k A_{k-1} x_{k-1} \\ &\quad + H_k B_{k-1} u_{k-1} + H_k w_{k-1} + v_k - H_k A_{k-1} \hat{x}_{k-1}^+ \\ &\quad - H_k B_{k-1} u_{k-1} - H_k \hat{w}_{k-1}) - f(\hat{x}_{k-1}^+, u_{k-1})] \\ &\quad (\text{from Eqs. 1, 2, and 13}) \\ &= E[\hat{w}_{k-1} + K_k H_k A_{k-1} \delta \tilde{x}_{k-1}^+ + K_k H_k \delta \tilde{w}_{k-1} + K_k v_k] \\ &= E[-w_{k-1} + w_{k-1} + \hat{w}_{k-1} + K_k H_k A_{k-1} \delta \tilde{x}_{k-1}^+ \\ &\quad + K_k H_k \delta \tilde{w}_{k-1} + K_k v_k] \\ &= E[w_{k-1} + K_k H_k A_{k-1} \delta \tilde{x}_{k-1}^+ + (K_k H_k - I) \delta \tilde{w}_{k-1} + K_k v_k] \quad (16) \end{aligned}$$

In this equation,  $\delta \tilde{x}^+ \in R_n$  and  $\delta \tilde{w} \in R_n$  are defined by  $\delta \tilde{x}^+ = x - \hat{x}^+$  and  $\delta \tilde{w} = w - \hat{w}$ , and denote the errors between the actual and estimated states and between the actual and estimated disturbances, respectively. If the state estimation and disturbance estimation are performed ideally, the expected values of the state and disturbance estimation errors can be assumed to be zero ( $E[\delta \tilde{x}^+] \approx 0$ ,  $E[\delta \tilde{w}] \approx 0$ ). The expected value of the measurement noise  $v_k$  is zero ( $E[v_k] = 0$ ) according to the KF definition; hence, Eq. (16) can be approximated as follows:

$$E[y_{w,k}] = E[\hat{x}_k^+ - f(\hat{x}_{k-1}^+, u_{k-1})] \approx E[w_{k-1}] \quad (17)$$

As indicated by Eq. (17), an expected value close to the actual disturbance ( $w$ ) can be obtained through the difference between the a posteriori state estimate and the model-based calculation part of the a priori state estimate. This verifies that the assumption in Eq. (15) is appropriate. Consequently, as shown in Fig. 3, the newly proposed Kalman filter framework can be expressed by combining the DLKF concept proposed in the present study with the disturbance measurement concept. A comparison between Figs. 2 and 3 shows that the state and disturbance estimators in Fig. 2 form separate KF loops.

As shown in Fig. 3, the disturbance estimate  $\hat{w}^+$  obtained through the disturbance-estimating KF on the lower right side is fed back into the state-estimating KF (upper left side), thereby correcting the error caused by model uncertainty in the prediction step of the state-estimating KF. This increases the precision of the model-based prediction. Furthermore, the final estimated value  $\hat{x}^+$  and the model-based prediction value  $f(\hat{x}^+, u)$  produced by the state-estimating KF are combined in the disturbance detector, producing the disturbance measurement value ( $y_w$ ) via Eq. (15); this value is then used in the correction step of the disturbance estimator. The tasks performed in the main blocks in Fig. 3 can be summarized as follows:

- State-estimating KF loop

$$\begin{aligned} \text{Prediction step : } & \hat{x}_k^- = f(\hat{x}_{k-1}^+, u_{k-1}) + \hat{w}_{k-1}^+ \\ & = A_{k-1}\hat{x}_{k-1}^+ + B_{k-1}u_{k-1} + \hat{w}_{k-1}^+ \end{aligned} \quad (18)$$

$$\text{Correction step : } \hat{x}_k^+ = \hat{x}_k^- + K_k(y_k - h(\hat{x}_k^-)) \quad (19)$$

- Disturbance-estimating KF loop

$$\text{Prediction step : } \hat{w}_k^- = f_w(\hat{w}_{k-1}^+) = A_{w,k-1}\hat{w}_{k-1}^+ \quad (20)$$

$$\text{Correction step : } \hat{w}_k^+ = \hat{w}_k^- + G_k(y_{w,k} - \hat{w}_k^-) \quad (21)$$

$$\begin{aligned} \text{Measurement : } & y_{w,k} = \hat{x}_k^+ - f(\hat{x}_{k-1}^+, u_{k-1}) \\ & = \hat{x}_k^+ - A_{k-1}\hat{x}_{k-1}^+ - B_{k-1}u_{k-1} \end{aligned} \quad (22)$$

In the above expressions,  $f_w(\cdot)$  and  $A_w$  are the state transition function/matrix used in the model prediction in the disturbance-estimating KF, which in our case is the identity matrix ( $I \in R_{n \times n}$ , which means there is no a priori information about the disturbance). Further,  $K_k$  and  $G_k$  are the Kalman gains of the state estimator and disturbance estimator, respectively. Their calculation is discussed in Section 3.2.

Forming a separate KF loop for state and disturbance offers several advantages. In the case of the Q-filter-based disturbance estimator used in previous studies [43–46], it was difficult to design an appropriate Q-filter. In particular, when the frequency characteristics of the disturbance or model uncertainty are not known in advance, it is difficult to find an appropriate Q-filter. In contrast, because the proposed KF-based disturbance estimator obtains the appropriate Kalman gain continuously according to the probability distribution, it is possible to estimate the disturbance more precisely. Furthermore, unlike the previous methods, the proposed DLKF does not require bounding conditions to the model uncertainty or the solution of Riccati equations. Further details are provided in Section 3.2.

Another significant advantage is that the correlation between state and disturbance does not need to be considered when setting the process and measurement noise covariance matrices, which are tuning parameters of the KF. If the estimator is created by augmenting both state and disturbance into a single augmented state vector, it is necessary to tune the level of correlation between the two elements during the noise covariance matrix ( $Q, R$ ) tuning step. In such a scheme, the parameter tuning process becomes very difficult as the system size ( $n$ ) increases. However, in the proposed DLKF scheme, the correlation between state and disturbance can be calculated automatically by the estimator if the noise covariance matrix corresponding to each Kalman filter loop is set independently. In other words, setting up the process/measurement noise covariance matrix in the early stages of the Kalman filter implementation is much simpler in the case of the proposed estimator than using an augmented state incorporating both state and disturbance into a single Kalman filter. Furthermore, the resulting matrix dimensions in the proposed method are lower than those of the augmentation method. The next subsection discusses the induction of equations to acquire the Kalman gain in the state estimating loop and disturbance estimating loop.

### 3.2. DLKF formulation

The equation of the original Kalman filter should not be used as is in the case of the proposed two Kalman filter loops. Because the results (or intermediate values) of the two estimators affect each other – in the prediction step of the state-estimating KF loop and in the correction step of the disturbance-estimating KF loop – the KF equations should be carefully modified to consider the resulting effects. In addition, correlation information between the state and disturbance should be considered. To proceed, some mathematical definitions are first established (see Table 1).

**Table 1**

Mathematical notation for deriving DLKF algorithm.

---

$x, w$ :	real system state, real model disturbance ( $\epsilon R_n$ )
$y, v$ :	system measurement, measurement noise ( $\epsilon R_m$ )
$u$ :	control input ( $\epsilon R_p$ )
$f(\cdot)$ :	state transition function / $h(\cdot)$ : measurement function
$A = \frac{\delta f}{\delta x} _{x=\bar{x}, u=\bar{u}}$ , $B = \frac{\delta f}{\delta u} _{x=\bar{x}, u=\bar{u}}$ , $H = \frac{\delta h}{\delta x} _{x=\bar{x}}$	
$\hat{x}^-, \hat{x}^+$ :	priori, posteriori state estimate ( $\epsilon R_n$ )
$\hat{w}^-, \hat{w}^+$ :	priori, posteriori disturbance estimate ( $\epsilon R_n$ )
$P^-, P^+$ :	priori, posteriori state estimate error covariance matrix ( $\epsilon R_{n \times n}$ )
$(P^- = E[(x_k - \hat{x}_k^-)(x_k - \hat{x}_k^-)^T])$	$P^+ = E[(x_k - \hat{x}_k^+)(x_k - \hat{x}_k^+)^T])$
$W^-, W^+$ :	priori, posteriori disturbance estimate error covariance matrix ( $\epsilon R_{n \times n}$ )
$(W^- = E[(w_k - \hat{w}_k^-)(w_k - \hat{w}_k^-)^T])$	$W^+ = E[(w_k - \hat{w}_k^+)(w_k - \hat{w}_k^+)^T])$
$K, G$ :	state, disturbance-estimating Kalman filter gain matrix
$C^-, C^+$ :	priori, posteriori state and disturbance error cross-covariance matrix
$(C^- = E[(x_k - \hat{x}_k^-)(w_k - \hat{w}_k^-)^T])$	$C^+ = E[(x_k - \hat{x}_k^+)(w_k - \hat{w}_k^+)^T])$
$\delta x = x - \bar{x}$ , $\delta y = y - \bar{y}$ , $\delta u = u - \bar{u}$ , $\delta w = w - \bar{w}$	
$\delta \hat{x}^* = \hat{x}^* - \bar{x}$ (superscript * can be + or -)	
$\delta \hat{w}^* = \hat{w}^* - \bar{w}$ (superscript * can be + or -)	
$\delta \tilde{x}^* = \delta x - \delta \hat{x}^* = x - \hat{x}^*$ : error of state estimate (superscript * can be + or -)	
$\delta \tilde{w}^* = \delta w - \delta \hat{w}^* = w - \hat{w}^*$ : error of disturbance estimate (superscript * can be + or -)	
Here, $\bar{x}, \bar{y}, \bar{u}$ , and $\bar{w}$ denote values on the nominal trajectory.	

---

The real system and its linearized equation can be expressed as follows:

$$x_k = f(x_{k-1}, u_{k-1}) + w_{k-1}$$

$$y_k = h(x_k) + v_k$$

$$\delta x_k = A_{k-1}\delta x_{k-1} + B_{k-1}\delta u_{k-1} + \delta w_{k-1} \quad (23)$$

$$\delta y_k = H_k\delta x_k + v_k \quad (24)$$

The state errors and disturbance errors at each step ( $\delta \tilde{x}^-, \delta \tilde{x}^+, \delta \tilde{w}^-$ ,  $\delta \tilde{w}^+$ ) can be calculated using Eqs. (18)–(24) as follows:

- Calculate  $\delta \tilde{x}^-$  and  $\delta \tilde{x}^+$ :  
From Eq. (18),

$$\delta \tilde{x}_k^- = A_{k-1}\delta \hat{x}_{k-1}^+ + B_{k-1}\delta u_{k-1} + \delta \hat{w}_{k-1}^+ \quad (25)$$

Subtracting Eq. (25) from Eq. (23) yields

$$\therefore \delta \tilde{x}_k^- = A_{k-1}\delta \hat{x}_{k-1}^+ + \delta \tilde{w}_{k-1}^- \quad (26)$$

From Eqs. (19) and (24),

$$\begin{aligned} \delta \hat{x}_k^+ &= \delta \hat{x}_k^- + K_k(\delta y_k - H_k\delta \hat{x}_k^-) \\ &= \delta \tilde{x}_k^- + K_k(H_k\delta \tilde{x}_k^- + v_k) \end{aligned} \quad (27)$$

Subtracting both sides of Eq. (27) from  $\delta x_k = \delta x_k$  yields

$$\therefore \delta \tilde{x}_k^+ = (I - K_k H_k) \delta \tilde{x}_k^- - K_k v_k \quad (28)$$

- Calculate  $\delta \tilde{w}^-$  and  $\delta \tilde{w}^+$ :  
From Eq. (20),

$$\delta \hat{w}_k^- = A_{w,k-1}\delta \hat{w}_{k-1}^+ \quad (29)$$

Subtracting Eq. (29) from  $\delta w_k = A_{w,k-1}\delta w_{k-1} + p$  yields

$$\therefore \delta \tilde{w}_k^- = A_{w,k-1}\delta \tilde{w}_{k-1}^+ + p \quad (30)$$

where  $p \in R_n$  is the process noise in the disturbance prediction model. Substituting Eq. (25) into Eq. (27) yields

$$\begin{aligned}\delta\hat{x}_k^+ &= A_{k-1}\delta\hat{x}_{k-1}^+ + B_{k-1}\delta u_{k-1} + \delta\hat{w}_{k-1}^+ + K_k(H_k\delta\tilde{x}_k^- + v_k) \\ \delta\hat{x}_k^+ - A_{k-1}\delta\hat{x}_{k-1}^+ - B_{k-1}\delta u_{k-1} &= \delta\hat{w}_{k-1}^+ + K_k(H_k\delta\tilde{x}_k^- + v_k)\end{aligned}\quad (31)$$

By plugging Eq. (22) into Eq. (21) and from Eq. (31),  $\delta\hat{w}_k^+$  can be arranged as follows:

$$\begin{aligned}\delta\hat{w}_k^+ &= \delta\hat{w}_k^- + G_k(\delta\hat{x}_k^+ - A_{k-1}\delta\hat{x}_{k-1}^+ - B_{k-1}\delta u_{k-1} + r - \delta\hat{w}_k^-) \\ &= \delta\hat{w}_k^- + G_k(\delta\hat{w}_{k-1}^+ + K_k(H_k\delta\tilde{x}_k^- + v_k) + r - \delta\hat{w}_k^-) \\ &= \delta\hat{w}_k^- + G_k(A_{w,k-1}^{-1}\delta\hat{w}_k^- + K_k(H_k\delta\tilde{x}_k^- + v_k) + r - \delta\hat{w}_k^-) \\ &\cong \delta\hat{w}_k^- + G_kK_k(H_k\delta\tilde{x}_k^- + v_k) + G_kr\end{aligned}\quad (32)$$

In the above equation,  $r \in R_n$  denotes the measurement noise in the disturbance-estimating KF. Subtracting both sides of Eq. (32) from  $\delta w_k = \delta\hat{w}_k$  yields

$$\therefore \delta\tilde{w}_k^+ = \delta\tilde{w}_k^- - G_kK_k(H_k\delta\tilde{x}_k^- + v_k) - G_kr \quad (33)$$

From the above procedure, the error equations of the priori/posteriori states and the disturbance can be obtained ( $\delta\tilde{x}^-$  = Eq. 26,  $\delta\tilde{x}^+$  = Eq. 28,  $\delta\tilde{w}^-$  = Eq. 30,  $\delta\tilde{w}^+$  = Eq. 33). Next, the Kalman gain ( $K_k$ ) of the state-estimating KF and the a priori/posteriori state estimate error covariance matrices ( $P_k^-$ ,  $P_k^+$ ) are calculated as follows:

- State estimator Kalman gain  $K_k$ :

$$\delta\tilde{y}_k = \delta y_k - \delta\hat{y}_k = H_k\delta x_k + v_k - H_k\delta\tilde{x}_k^- = H_k\delta\tilde{x}_k^- + v_k \quad (34)$$

Multiplying  $\delta\tilde{x}_k^+$  (Eq. (28)) by the transpose of  $\delta\tilde{y}_k$  (Eq. (34)) yields

$$\begin{aligned}\delta\tilde{x}_k^+\delta\tilde{y}_k^T &= ((I - K_kH_k)\delta\tilde{x}_k^- - K_kv_k)(\delta\tilde{x}_k^{-T}H_k^T + v_k^T) \\ &= (I - K_kH_k)\delta\tilde{x}_k^-\delta\tilde{x}_k^{-T}H_k^T + (I - K_kH_k)\delta\tilde{x}_k^-v_k^T \\ &\quad - K_kv_k\delta\tilde{x}_k^{-T}H_k^T - K_kv_kv_k^T\end{aligned}\quad (35)$$

As in the original KF, by assuming that the covariance of the state error and the state-estimating KF's innovation is zero,  $E[\delta\tilde{x}_k^+\delta\tilde{y}_k^T] = 0$  is satisfied and the following equation can be obtained by using Eq. (35). Here, the covariance of  $\delta\tilde{x}^-$  and  $v$  is assumed as zero ( $E[\delta\tilde{x}^-v^T] = 0$ ).

$$\begin{aligned}(I - K_kH_k)P_k^-H_k^T - K_kR_k &= 0 \\ \therefore K_k &= P_k^-H_k^T(H_kP_k^-H_k^T + R_k)^{-1}\end{aligned}\quad (36)$$

- A priori state estimate error covariance matrix  $P_k^-$ :

From  $P_k^- = E[\delta\tilde{x}_k^+\delta\tilde{x}_k^{-T}]$  and Eq. (26),

$$\begin{aligned}\delta\tilde{x}_k^-\delta\tilde{x}_k^{-T} &= (A_{k-1}\delta\tilde{x}_{k-1}^+ + \delta\tilde{w}_{k-1}^+)(\delta\tilde{x}_{k-1}^{+T}A_{k-1}^T + \delta\tilde{w}_{k-1}^{+T}) \\ &= A_{k-1}\delta\tilde{x}_{k-1}^+\delta\tilde{x}_{k-1}^{-T}A_{k-1}^T + A_{k-1}\delta\tilde{x}_{k-1}^+\delta\tilde{w}_{k-1}^{+T} \\ &\quad + \delta\tilde{w}_{k-1}^+\delta\tilde{x}_{k-1}^{-T}A_{k-1}^T + \delta\tilde{w}_{k-1}^+\delta\tilde{w}_{k-1}^{+T}\end{aligned}\quad (37)$$

$$\therefore P_k^- = E[\delta\tilde{x}_k^-\delta\tilde{x}_k^{-T}] = A_{k-1}P_{k-1}^+A_{k-1}^T + A_{k-1}C_{k-1}^+ + C_{k-1}^+A_{k-1}^T + W_{k-1}^+ \quad (38)$$

- A posteriori state estimate error covariance matrix  $P_k^+$ :

From  $P_k^+ = E[\delta\tilde{x}_k^+\delta\tilde{x}_k^{-T}]$  and Eq. (28),

$$\begin{aligned}\delta\tilde{x}_k^+\delta\tilde{x}_k^{-T} &= ((I - K_kH_k)\delta\tilde{x}_k^- - K_kv_k)(\delta\tilde{x}_k^{-T}(I - K_kH_k)^T - v_k^TK_k^T) \\ &= (I - K_kH_k)\delta\tilde{x}_k^-\delta\tilde{x}_k^{-T}(I - K_kH_k)^T \\ &\quad - (I - K_kH_k)v_k^TK_k^T + K_kv_kv_k^T\end{aligned}\quad (39)$$

$$P_k^+ = E[\delta\tilde{x}_k^+\delta\tilde{x}_k^{-T}] = (I - K_kH_k)P_k^-(I - K_kH_k)^T + K_kR_kK_k^T$$

Substituting Eq. (36) into the above equation yields

$$\therefore P_k^+ = (I - K_kH_k)P_k^- \quad (40)$$

Next, the Kalman gain ( $G_k$ ) of the disturbance-estimating KF and the a priori/posteriori disturbance estimate error covariance matrices ( $W_k^-$ ,  $W_k^+$ ) are calculated according to their definitions, as follows:

- Disturbance estimator Kalman gain  $G_k$ :

$$\delta\tilde{y}_{w,k} = K_kH_k\delta\tilde{x}_k^- + K_kv_k + r \quad (41)$$

Multiplying  $\delta\tilde{w}_k^+$  (Eq. (33)) by the transpose of  $\delta\tilde{y}_{w,k}$  (Eq. (41)) yields

$$\begin{aligned}\delta\tilde{w}_k^+\delta\tilde{y}_{w,k}^T &= (\delta\tilde{w}_k^- - G_kK_kH_k\delta\tilde{x}_k^- - G_kK_kv_k - G_kr)(\delta\tilde{x}_k^{-T}H_k^TK_k^T \\ &\quad + v_k^TK_k^T + r^T) \\ &= \delta\tilde{w}_k^-\delta\tilde{x}_k^{-T}H_k^TK_k^T - G_kK_kH_k\delta\tilde{x}_k^-\delta\tilde{x}_k^{-T}H_k^TK_k^T \\ &\quad - G_kK_kv_k\delta\tilde{x}_k^{-T}H_k^TK_k^T - G_kr\delta\tilde{x}_k^{-T}H_k^TK_k^T \\ &\quad + \delta\tilde{w}_k^-\delta\tilde{x}_k^{-T}H_k^T - G_kK_kH_k\delta\tilde{x}_k^-v_k^TH_k^T - G_kK_kv_kv_k^TH_k^T \\ &\quad - G_kv_kv_k^TH_k^T + \delta\tilde{w}_k^-r^T - G_kK_kH_k\delta\tilde{x}_k^-r^T \\ &\quad - G_kK_kv_k^T - G_krr^T\end{aligned}\quad (42)$$

Given that the covariance of the disturbance error and the disturbance-estimating KF's innovation is zero,  $E[\delta\tilde{w}_k^+\delta\tilde{y}_{w,k}^T] = 0$  is satisfied. Further, assuming that the covariances between  $\delta\tilde{w}^-$  and  $v$ ,  $\delta\tilde{w}^-$  and  $r$ ,  $\delta\tilde{x}^-$  and  $r$ , and  $v$  and  $r$  are zero ( $E[\delta\tilde{w}^-v^T] = E[\delta\tilde{w}^-r^T] = E[\delta\tilde{x}^-r^T] = E[vr^T] = 0$ ), Eq. (42) can be expressed as follows. (Here, we assume that the noise covariance matrix of the disturbance measurement is  $R_r = E[rr^T]$ .)

$$\begin{aligned}C_k^{-T}H_k^TK_k^T - G_kK_kH_kP_k^-H_k^TK_k^T - G_kK_kR_kK_k^T - G_kR_r &= 0 \\ \therefore G_k &= C_k^{-T}H_k^TK_k^T(K_kH_kP_k^-H_k^TK_k^T + K_kR_kK_k^T + R_r)^{-1}\end{aligned}\quad (43)$$

- A priori disturbance estimate error covariance matrix  $W_k^-$ :

From  $W_k^- = E[\delta\tilde{w}_k^-\delta\tilde{w}_k^{-T}]$  and Eq. (30),

$$\begin{aligned}\delta\tilde{w}_k^-\delta\tilde{w}_k^{-T} &= (A_{w,k-1}\delta\tilde{w}_{k-1}^+ + p)(\delta\tilde{w}_{k-1}^{+T}A_{w,k-1}^T + p^T) \\ &= A_{w,k-1}\delta\tilde{w}_{k-1}^+\delta\tilde{w}_{k-1}^{+T}A_{w,k-1}^T \\ &\quad + A_{w,k-1}\delta\tilde{w}_{k-1}^+p^T + p\delta\tilde{w}_{k-1}^{+T}A_{w,k-1}^T + pp^T\end{aligned}\quad (44)$$

Let us assume that the covariances between  $\delta\tilde{w}^+$  and  $p$ , and between  $\delta\tilde{x}^+$  and  $p$  are zero ( $E[\delta\tilde{w}^+p^T] = E[\delta\tilde{x}^+p^T] = 0$ ). Given that  $Q_p$  is the model noise covariance ( $Q_p = E[pp^T]$ ) of the disturbance Kalman filter, the following equation is then satisfied.

$$\therefore W_k^- = E[\delta\tilde{w}_k^-\delta\tilde{w}_k^{-T}] = A_{w,k-1}W_{k-1}^+A_{w,k-1}^T + Q_p \quad (45)$$

- A posteriori disturbance estimate error covariance matrix  $W_k^+$ :

From  $W_k^+ = E[\delta\tilde{w}_k^+\delta\tilde{w}_k^{+T}]$  and Eq. (33),

$$\begin{aligned}\delta\tilde{w}_k^+\delta\tilde{w}_k^{+T} &= (\delta\tilde{w}_k^- - G_kK_k(H_k\delta\tilde{x}_k^- + v_k) - G_kr)(\delta\tilde{w}_k^{-T} \\ &\quad - (H_k\delta\tilde{x}_k^- + v_k)^TK_k^TG_k^T - r^TG_k^T) \\ &= \delta\tilde{w}_k^-\delta\tilde{x}_k^{-T}H_k^T + v_k^TK_k^TG_k^T \\ &\quad - \delta\tilde{w}_k^-\delta\tilde{x}_k^{-T}H_k^T - G_kK_k(H_k\delta\tilde{x}_k^- + v_k)\delta\tilde{x}_k^{-T}H_k^T \\ &\quad + G_kK_k(H_k\delta\tilde{x}_k^- + v_k)(\delta\tilde{x}_k^{-T}H_k^T + v_k^T)K_k^TG_k^T \\ &\quad + G_kK_k(H_k\delta\tilde{x}_k^- + v_k)r^TG_k^T \\ &\quad - G_kr\delta\tilde{x}_k^{-T}H_k^T + G_kr(\delta\tilde{x}_k^{-T}H_k^T + v_k^T)K_k^TG_k^T \\ &\quad + G_krr^TG_k^T\end{aligned}\quad (46)$$

$$\begin{aligned}
W_k^+ &= E[\tilde{w}_k^+ \delta \tilde{w}_k^{+T}] \\
&= W_k^- - C_k^{-T} H_k^T K_k^T G_k^T - G_k K_k H_k C_k^- \\
&\quad + G_k K_k (H_k P_k^- H_k^T + R_k) K_k^T G_k^T + G_k R_r G_k^T \\
\therefore W_k^+ &= W_k^- - G_k K_k H_k C_k^- - C_k^{-T} H_k^T K_k^T G_k^T \\
&\quad + G_k P_k^- H_k^T K_k^T G_k^T + G_k R_r G_k^T \quad (47)
\end{aligned}$$

As mentioned in Eq. (12), the state and disturbance are correlated with each other. Therefore, the state and disturbance error cross-covariance matrices (priori:  $C_k^-$ , posteriori:  $C_k^+$ ) should be considered, because they provide information about the covariance between the state estimate error and the disturbance estimate error.

- A priori state-disturbance error cross-covariance matrix  $C_k^-$ :

From  $C_k^- = E[\delta \tilde{x}_k^- \delta \tilde{w}_k^{-T}]$  and Eqs. (26) and (30),

$$\begin{aligned}
\delta \tilde{x}_k^- \delta \tilde{w}_k^{-T} &= (A_{k-1} \delta \tilde{x}_{k-1}^+ + \delta \tilde{w}_{k-1}^+) (\delta \tilde{w}_{k-1}^{+T} A_{w,k-1}^T + p^T) \\
&= A_{k-1} \delta \tilde{x}_{k-1}^+ \delta \tilde{w}_{k-1}^{+T} A_{w,k-1}^T + A_{k-1} \delta \tilde{x}_{k-1}^+ p^T \\
&\quad + \delta \tilde{w}_{k-1}^+ \delta \tilde{w}_{k-1}^{+T} A_{w,k-1}^T + \delta \tilde{w}_{k-1}^{+T} p^T \quad (48)
\end{aligned}$$

$$\begin{aligned}
\therefore C_k^- &= E[\delta \tilde{x}_k^- \delta \tilde{w}_k^{-T}] = A_{k-1} C_{k-1}^+ A_{w,k-1}^T \\
&\quad + W_{k-1}^+ A_{w,k-1}^T \quad (49)
\end{aligned}$$

- A posteriori state-disturbance error cross-covariance matrix  $C_k^+$ :

From  $C_k^+ = E[\delta \tilde{x}_k^+ \delta \tilde{w}_k^{+T}]$  and Eqs. (28) and (33),

$$\begin{aligned}
\delta \tilde{x}_k^+ \delta \tilde{w}_k^{+T} &= ((I - K_k H_k) \delta \tilde{x}_k^- - K_k v_k) (\delta \tilde{w}_k^{-T} \\
&\quad - (H_k \delta \tilde{x}_k^- + v_k)^T K_k^T G_k^T - r^T G_k^T) \\
&= (I - K_k H_k) \delta \tilde{x}_k^- \delta \tilde{w}_k^{-T} \\
&\quad - (I - K_k H_k) \delta \tilde{x}_k^- (\delta \tilde{x}_k^{-T} H_k^T + v_k^T) K_k^T G_k^T \\
&\quad - (I - K_k H_k) \delta \tilde{x}_k^- r^T G_k^T \\
&\quad - K_k v_k \delta \tilde{w}_k^{-T} + K_k v_k (\delta \tilde{x}_k^{-T} H_k^T + v_k^T) K_k^T G_k^T \\
&\quad + K_k v_k r^T G_k^T \quad (50) \\
\therefore C_k^+ &= E[\delta \tilde{x}_k^+ \delta \tilde{w}_k^{+T}] = (I - K_k H_k) C_k^- \\
&\quad - (I - K_k H_k) P_k^- H_k^T K_k^T G_k^T + K_k R_k K_k^T G_k^T \quad (51)
\end{aligned}$$

By calculating both the a priori and a posteriori cross-covariances, the level of correlation between state and disturbance can be accurately estimated with respect to that of [46]. Finally, using Eqs. (18)–(22), (36), (38), (40), (43), (45), (47), (49), and (51), the proposed DLKF can be arranged in a discrete/recursive form. Table 2 shows the final obtained result.

The state Kalman gain ( $K_k$ ) and disturbance Kalman gain ( $G_k$ ) are calculated using the equations in Steps 3 and 9, respectively. Even though each one of these equations requires a matrix-inversion, they are always invertible, because the terms in parentheses are always positive definite. Therefore, the need for matrix-inversion does not result in any numerical issues. However, during the actual implementation, ill-conditioning problems can arise because of the calculation's precision limitations. To enhance numerical stability during the discrete computation process, the symmetry properties of the state and disturbance estimate error covariance matrices ( $P_k^+$  and  $W_k^+$ , respectively) should be maintained. To achieve these, a small trick can be used. After Steps 5 and 11 in Table 2, two equations  $P_k^+ = 0.5(P_k^+ + P_k^{+T})$  and  $W_k^+ = 0.5(W_k^+ + W_k^{+T})$  can be used to ensure symmetry. In addition, for the symmetric a posteriori state estimate error covariance ( $P_k^+$ ), a Joseph form

**Table 2**  
Final recursive equations of DLKF.

**Process #1: State Estimation**

- (1) State prediction step  
 $\hat{x}_k = f(\hat{x}_{k-1}, u_{k-1}) + \hat{w}_{k-1}^+$
- (2) Calculate priori state estimate error covariance matrix  
 $P_k^- = A_{k-1} P_{k-1}^+ A_{k-1}^T + A_{k-1} C_{k-1}^+ + C_{k-1}^{+T} A_{k-1}^T + W_{k-1}^+$
- (3) Calculate state Kalman gain  
 $K_k = P_k^- H_k^T (H_k P_k^- H_k^T + R_k)^{-1}$
- (4) State estimate correction step  
 $\hat{x}_k^+ = \hat{x}_k^- + K_k (y_k - h(\hat{x}_k^-))$
- (5) Update state estimate error covariance matrix  
 $P_k^+ = (I - K_k H_k) P_k^-$

**Process #2: Disturbance Estimation**

- (6) Disturbance prediction step  
 $\hat{w}_k^- = f_w(\hat{w}_{k-1}^+)$
- (7) Calculate priori disturbance estimate error covariance matrix  
 $W_k^- = A_{w,k-1} W_{k-1}^+ A_{w,k-1}^T + Q_p$
- (8) Calculate priori estimate error cross-covariance matrix  
 $C_k^- = A_{k-1} C_{k-1}^+ A_{w,k-1}^T + W_{k-1}^+ A_{w,k-1}^T$
- (9) Calculate disturbance Kalman gain  
 $G_k = C_k^{-T} H_k^T K_k^T (K_k H_k P_k^- H_k^T + K_k R_k K_k^T + R_r)^{-1}$
- (10) Disturbance estimate correction step  
 $\hat{w}_k^+ = \hat{w}_k^- + G_k (y_{w,k} - \hat{w}_k^-)$  (when:  $y_{w,k} = \hat{x}_k^+ - f(\hat{x}_{k-1}^+, u_{k-1})$ )
- (11) Update disturbance estimate error covariance matrix  
 $W_k^+ = W_k^- - G_k K_k H_k C_k^- - C_k^{-T} H_k^T K_k^T G_k^T + G_k P_k^- H_k^T K_k^T G_k^T + G_k R_k G_k^T$
- (12) Update estimate error cross-covariance matrix  
 $C_k^+ = (I - K_k H_k) C_k^- - (I - K_k H_k) P_k^- H_k^T K_k^T G_k^T + K_k R_k K_k^T G_k^T$

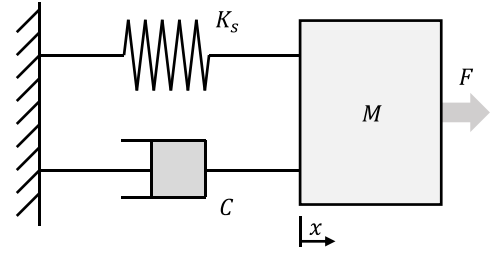


**Fig. 4.** Mass-spring-damper system for verification of proposed DLKF. Physical parameters:  $M = 50$  (kg),  $K_s = 500$  (N/m),  $C = 20$  (Ns/m).

$(P_k^+ = (I - K_k H_k) P_k^- (I - K_k H_k)^T + K_k R_k K_k^T$ , [38]) is preferred to  $P_k^+ = (I - K_k H_k) P_k^-$ .

### 3.3. Simple linear model example

This subsection uses a simple example to demonstrate the performance of the DLKF proposed in Section 3.1 and mathematically specified in Section 3.2. In addition, the results are compared with those obtained with other Kalman filters. The simple mass-spring-damper model shown in Fig. 4 is used in the example.

The physical parameters used in the test are shown in Fig. 4. The parameters are intuitively chosen, without any further criteria of choice. The designed estimator provides estimates of the mass motion (position and velocity) when a force (known input:  $u$ ) is applied. The estimator model is based on the equation of motion of the mass-spring-damper system, and the virtually measured position and velocity (with additive white Gaussian noise) are regarded as measurements ( $E[vv^T] = \text{diag}(0.0010.001)$ ). This system can be expressed by the following simple differential equation.

$$M\ddot{x} = F - C\dot{x} - K_s x \quad (52)$$

Let us assume that the state to be followed is  $x = [\text{position } \text{velocity}]^T = [x \dot{x}]^T \in R_2$ . Based on Eq. (52), the state, input, and measurement transition matrices for the Kalman filter configuration are

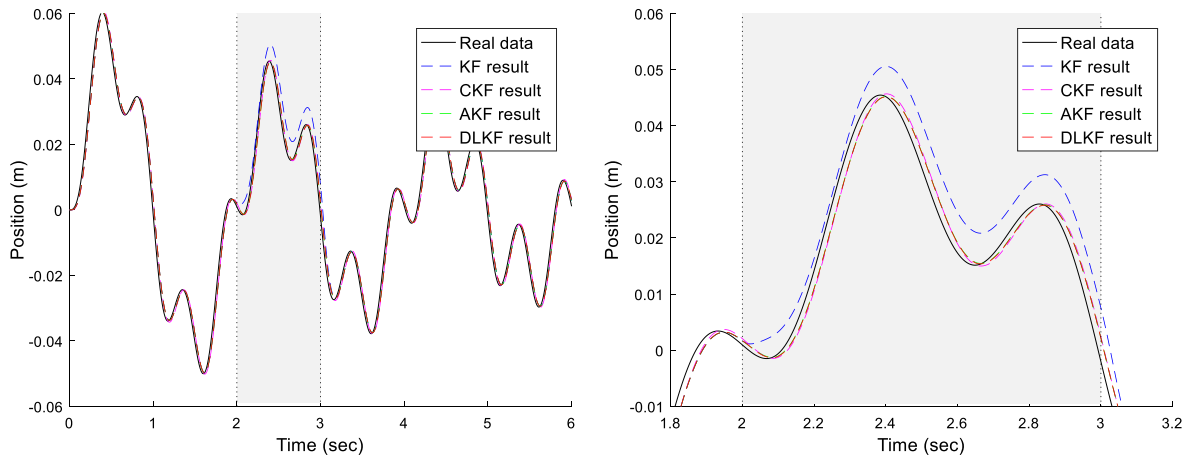


**Fig. 5.** Position estimation result of each Kalman filter. The gray region represents the section with the modeling error. Without the modeling error, all the KFs showed good estimation results. However, when the modeling error occurred, the estimation performance of the general KFs was significantly degraded. The figure on the right is an enlargement of the left figure in the time domain.

expressed as follows (here,  $\Delta t = 0.001$  s is the discrete time gap).

$$\begin{aligned} x_{k+1} &= Ax_k + Bu_k, \quad y_k = Hx_k, \quad x = [x \dot{x}]^T, \quad u_k = F(k \cdot \Delta t), \\ A &= \begin{bmatrix} 1 & \Delta t \\ -K_s \cdot \Delta t/M & 1 - C \cdot \Delta t/M \end{bmatrix}, \quad B = \begin{bmatrix} 0 \\ \Delta t/M \end{bmatrix}, \\ H &= \begin{bmatrix} 1 & 0 \\ 0 & 1 \end{bmatrix} \end{aligned} \quad (53)$$

In this example, a sinusoidal force was applied to the mass (frequency, 5 Hz; amplitude, 100 N). In order to compare the performance of the newly proposed DLKF with that of other types of KFs, the following four state-estimating KFs were configured using Eq. (53).

- KF: Original/conventional Kalman filter
- CKF: Combined KF based on [46] (KF + Q-filtered disturbance feedback)
- AKF: Augmented KF, i.e., single Kalman filter with an augmented state (original state + disturbance)
- DLKF: Proposed dual-loop KF estimator.

For a fair performance comparison, the same value was used for the noise covariance matrix ( $Q, R, Q_p, R_r$ ) used in all the KFs ( $Q = \text{diag}(0.1, 0.01), R = \text{diag}(20, 20), Q_p = \text{diag}(0.01, 1), R_r = (5, 1)$ ). In order to examine the estimation performance of each KF in the presence of a modeling error, the state transition matrix  $A(t)$  was deliberately changed into an incorrect model matrix when  $2 \leq t \leq 3$ . During this time, the mass and spring stiffness were intentionally distorted (Mass and damping coefficient information were distorted by 20%, and spring constant was distorted by 50%). Thus, an error ( $A_{\text{disturbance}}$ ) was introduced into the model as follows.

$$A(t) = \begin{cases} A_{\text{real}} & \text{when } t < 2 \text{ or } t > 3 \\ A_{\text{real}} + A_{\text{disturbance}} & \text{when } 2 \leq t \leq 3 \end{cases} \quad (54)$$

Fig. 5 shows the estimation results obtained with each filter. The gray region in the figure ( $2 \leq t \leq 3$ ) represents the section where the modeling error was introduced, as per Eq. (54). The black solid line represents the actual mass position value. As shown, the four KFs showed good position estimation results in the sections without modeling errors. However, the conventional KF could not estimate the position well in the case of a model disturbance. The error in the position value is shown in Fig. 6. As shown, the performance of the conventional KF (blue line) was significantly degraded in the section where the modeling error occurred, compared with the sections where there were no modeling errors. The

**Table 3**  
Comparison of the four types of filters in terms of computation time and accuracy.

Type	Computation time		Maximum error	
	Time (μs)	Ratio	Value (mm)	Ratio
KF	37	1	5.48	68.5
CKF	90	2.43	0.61	7.6
AKF	48	1.30	0.25	3.1
DLKF	98	2.64	0.08	1

reason is that a disturbance ( $w$ ) in the prediction step occurred because the modeling error ( $\Delta A$ ) was not zero-mean, white, Gaussian noise. This violates the optimality condition of the conventional KF. Under such circumstances, the proposed DLKF (red line) showed the best estimation results.

On the other hand, the CKF proposed in [46] showed a degraded estimation performance when compared to the DLKF. This is because an optimal Q-filter (or low-pass filter) implementation according to the changing circumstances is not possible. Although the AKF showed a reasonable performance, it is not as robust to the disturbance as the DLKF. For the DLKF, the correlation between state and disturbance is calculated automatically by a closed-form equation; however, for the AKF, the covariance between them should be tuned by the designer, which is a drawback of this method. Table 3 presents the above-mentioned results numerically. The absolute computation time was measured in a MATLAB® R2016 environment, with an Intel® Core™ i7 CPU. The proposed DLKF showed more robust and accurate state estimation performance than the previously proposed KFs in the presence of a modeling error.

### 3.4. Feature analysis

This subsection evaluates the performance of the newly designed KF framework through frequency analysis, as in [44]. The analysis was performed using two estimators: the original KF and the proposed DLKF. In this analysis, the sensitivity of the estimation error ( $e = x - \hat{x}^+ = \delta\tilde{x}^+$ ) with respect to the process disturbance ( $w$ ) and measurement noise ( $v$ ) was analyzed using the respective z-domain transfer functions. Here, for simplicity and clarity, we only present the transfer function formulation. A detailed derivation can be performed using the equations given in Section 3.2.

- Conventional Kalman filter

$$\delta\tilde{x}_k^- = A\delta\tilde{x}_{k-1}^+ + w_{k-1} \quad (55)$$

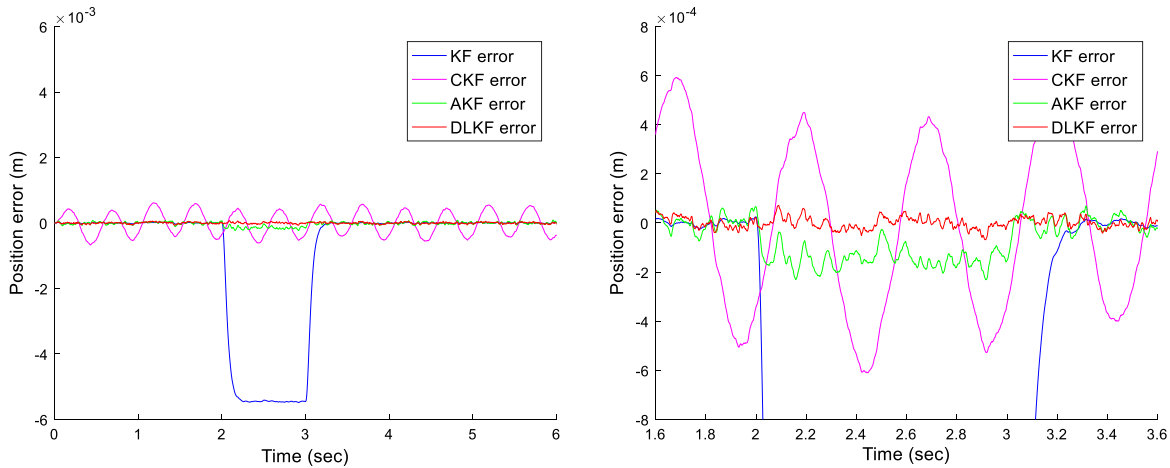


**Fig. 6.** Position estimation error result of each Kalman filter. The proposed DLKF showed the best estimation result in the section ( $2 \leq t \leq 3$ ) with a modeling error. The figure on the right is an enlargement of the left figure in the time domain.

$$\delta\tilde{x}_k^+ = \delta\tilde{x}_k^- - KH\delta\tilde{x}_k^- - Kv_k \quad (56)$$

By substituting Eq. (55) into Eq. (56) and arranging the resulting equation, the following equation is obtained.

$$\delta\tilde{x}_{k+1}^+ = (A - KHA)\delta\tilde{x}_k^+ + (I - KH)w_k - Kv_{k+1} \quad (57)$$

Applying the z-transform and arranging Eq. (57), the following equation can be obtained.

$$\therefore \tilde{X} = (zI - A + KHA)^{-1} [I - KH \quad -Kz] \begin{bmatrix} W \\ V \end{bmatrix} \quad (58)$$

- Dual-loop Kalman filter

$$\delta\tilde{x}_k^- = A\delta\tilde{x}_{k-1}^+ + \delta\tilde{w}_{k-1}^+ \quad (59)$$

$$\delta\tilde{x}_k^+ = \delta\tilde{x}_k^- - KH\delta\tilde{x}_k^- - Kv_k \quad (60)$$

By substituting Eq. (59) into Eq. (60) and rearranging the resulting equation, the following equation is obtained.

$$\delta\tilde{x}_{k+1}^+ = (A - KHA)\delta\tilde{x}_k^+ + (I - KH)\delta\tilde{w}_k^+ - Kv_{k+1} \quad (61)$$

The equation of the posteriori disturbance estimate error is obtained as follows:

$$\begin{aligned} \delta\tilde{w}_{k+1}^+ &= (-GKHA)\delta\tilde{x}_k^+ + (I - GKH)\delta\tilde{w}_k^+ + w_{k+1} \\ &\quad - w_k + (-GK)v_{k+1} \end{aligned} \quad (62)$$

By applying the z-transform and augmenting Eqs. (61) and (62), the following equation is obtained.

$$\begin{aligned} \therefore \begin{bmatrix} \tilde{X} \\ \tilde{W} \end{bmatrix} &= \left( zI - \begin{bmatrix} A - KHA & I - KH \\ -GKHA & I - GKH \end{bmatrix} \right)^{-1} \begin{bmatrix} 0 & -Kz \\ zI - I & -GKz \end{bmatrix} \begin{bmatrix} W \\ V \end{bmatrix} \end{aligned} \quad (63)$$

Using the z-domain transfer functions in Eqs. (58) and (63), the frequency characteristics of the estimation error according to the disturbance ( $\tilde{X}/W$ ) or measurement noise ( $\tilde{X}/V$ ) can be determined when either the conventional KF or the DLKF are used. The system used in the analysis was the mass-spring-damper system described in Section 3.3. Therefore, matrices  $A$  and  $H$  are the same ones used in Eq. (53). The Kalman gains  $K$  (state estimator gain) and  $G$  (disturbance estimator gain) needed in the analysis

were calculated by solving the discrete algebraic Riccati equation (DARE) using the steady-state Kalman filter (SSKF) concept. The transfer function obtained above were analyzed using Bode plots, as shown in Figs. 7 and 8.

The Bode plot on the left side of Fig. 7 shows the magnitude frequency response of the position estimation error ( $\delta\tilde{x}^+ = x - \hat{x}^+$ ) relative to a position disturbance ( $w_1$ ) in the system model. The graph on the right side shows the magnitude frequency response of the position estimation error ( $\delta\tilde{x}^+$ ) relative to a velocity model disturbance ( $w_2$ ). As shown in the figures, the original KF is sensitive to low-frequency model disturbances, and therefore presents a large estimation error. Without loss of generality, low-frequency disturbances can be assumed to be smoothly biased noise, which is therefore non-zero-mean noise. In this noise condition, the original KF loses its optimality characteristics. On the other hand, the proposed DLKF shows an effective suppression of such disturbances. In particular, the advantage of the DLKF is evident in the low-frequency band. Fig. 8 shows the estimation error behavior relative to the measurement noise ( $v$ ). The left side of Fig. 8 shows the frequency response of the position estimation error with respect to position measurement noise. Although the performances of the two KFs are comparable in the low-frequency band, the DLKF is slightly more sensitive to high-frequency measurement noise than the original KF.

All these DLKF's properties result from the fact that the DLKF's disturbance compensation acts like a residual-error-integration compensator. This results in an effect similar to the I-control of proportional-integral-derivative (PID) control. Because of this, an oscillatory behavior can be observed during the DLKF parameter tuning process. This shortcoming can be overcome by using a second-order low-pass filter in the measurement process.

The convergence of the state estimation error can be examined through eigenvalues analysis. The convergence of the estimation error ( $\delta\tilde{x}^+ = x - \hat{x}^+$ ) of each KF can be examined through the eigenvalues of  $A - K \cdot H \cdot A$  ( $\lambda_1$ ) and  $I - K \cdot H$  ( $\lambda_2$ ) in Eq. (57) and (61). The eigenvalue of each KF is given below.

$$\begin{aligned} \lambda_{1,KF} &= \text{eig}(A - KHA)_{KF} = 0.9327, 0.9755 \\ \lambda_{2,KF} &= \text{eig}(I - KH)_{KF} = 0.9312, 0.9774 \\ \lambda_{1,DLKF} &= \text{eig}(A - KHA)_{DLKF} = 0.8207, 0.3057 \\ \lambda_{2,DLKF} &= \text{eig}(I - KH)_{DLKF} = 0.3058, 0.8207 \end{aligned} \quad (64)$$

In the results of Eq. (64), both filters have eigenvalues smaller than one (inside the unit circle). Therefore, both estimators can be said to be stable estimators for this system. In addition, it is noteworthy that the DLKF shows a faster convergence rate (smaller eigenvalue) than the traditional KF.

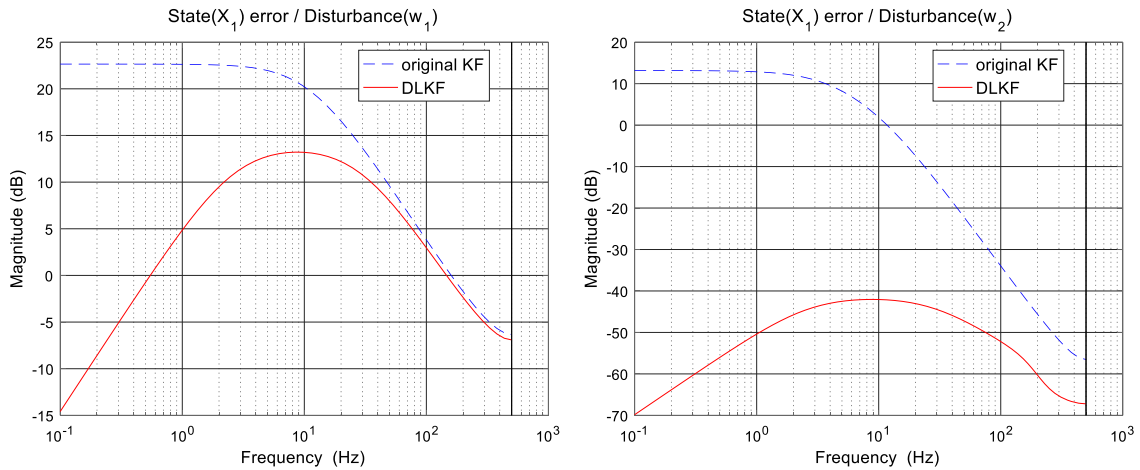


**Fig. 7.** (Left) Magnitude characteristics of position estimation error with respect to position model disturbance  $w_1$  (Right) Magnitude characteristics of position estimation error with respect to velocity model disturbance  $w_2$ . Compared with the conventional KF, the DLKF showed better performance.

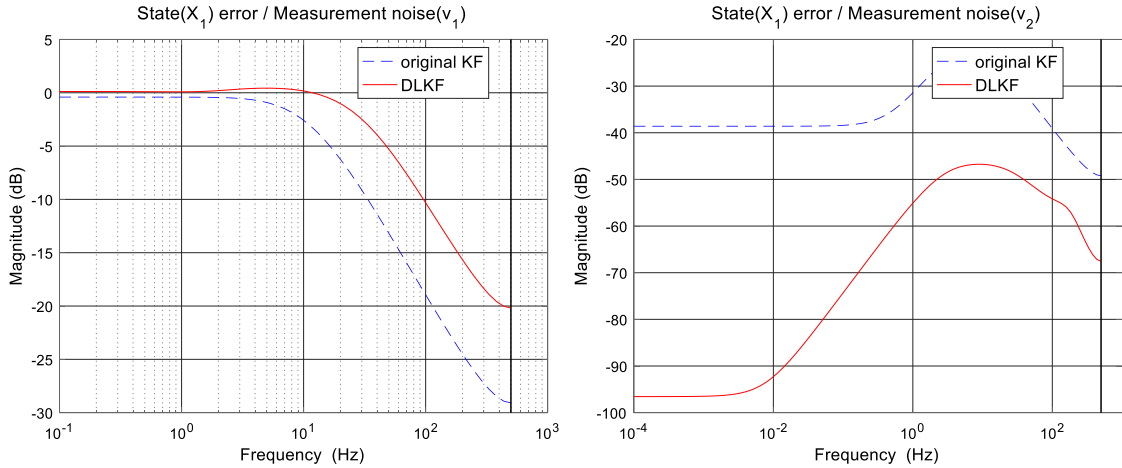


**Fig. 8.** (Left) Magnitude characteristics of position estimation error with respect to position measurement noise  $v_1$ . Comparable performance is observed in the low-frequency band, whereas the performance of the DLKF is lower in the high-frequency band. (Right) Magnitude characteristics of position estimation error with respect to velocity measurement noise  $v_2$ .

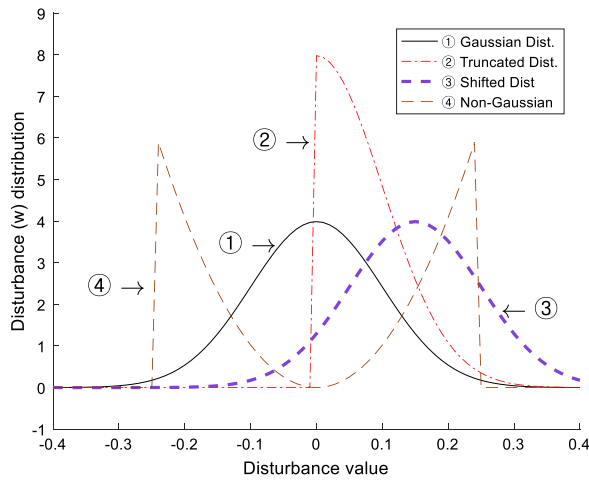


**Fig. 9.** Performance evaluation with regard to four types of disturbances. Probability distribution graph of each disturbance.

Additional tests were conducted to verify the estimation performance with regard to various types of disturbances. As shown in Fig. 9, four types of disturbances, namely normal-Gaussian

distribution (①), truncated-Gaussian distribution (②), shifted-Gaussian distribution (③), and non-Gaussian distribution (④) were applied to the previous mass-spring-damper system. The imposed noise parameters, such as mean and standard deviation, are shown in Fig. 9. The estimation results and the errors can be seen in Fig. 10, for each type of disturbance. When a disturbance is applied in the form of a zero-mean Gaussian distribution, satisfactory estimation results (unbiased) can be obtained using the original KF. This is expected, because the KF is the optimal estimator when the model and measurement noises are zero-mean, white, uncorrelated, and Gaussian distributed. However, when non-zero mean/non-Gaussian disturbances are applied, the performance of the original KF is degraded. In those cases, the original KF produces biased estimate results. In contrast, the proposed DLKF shows better estimation performance for the various types of non-zero mean/non-Gaussian disturbances. This is because of its adequate disturbance estimation and compensation scheme.

### 3.5. Nonlinear system estimation

As mentioned during the derivation process (Section 3.2), the proposed DLKF also can be applied in nonlinear system state estimation problems (similarly to the EKF). In most nonlinear system cases, the EKF produces sufficiently accurate estimation results.

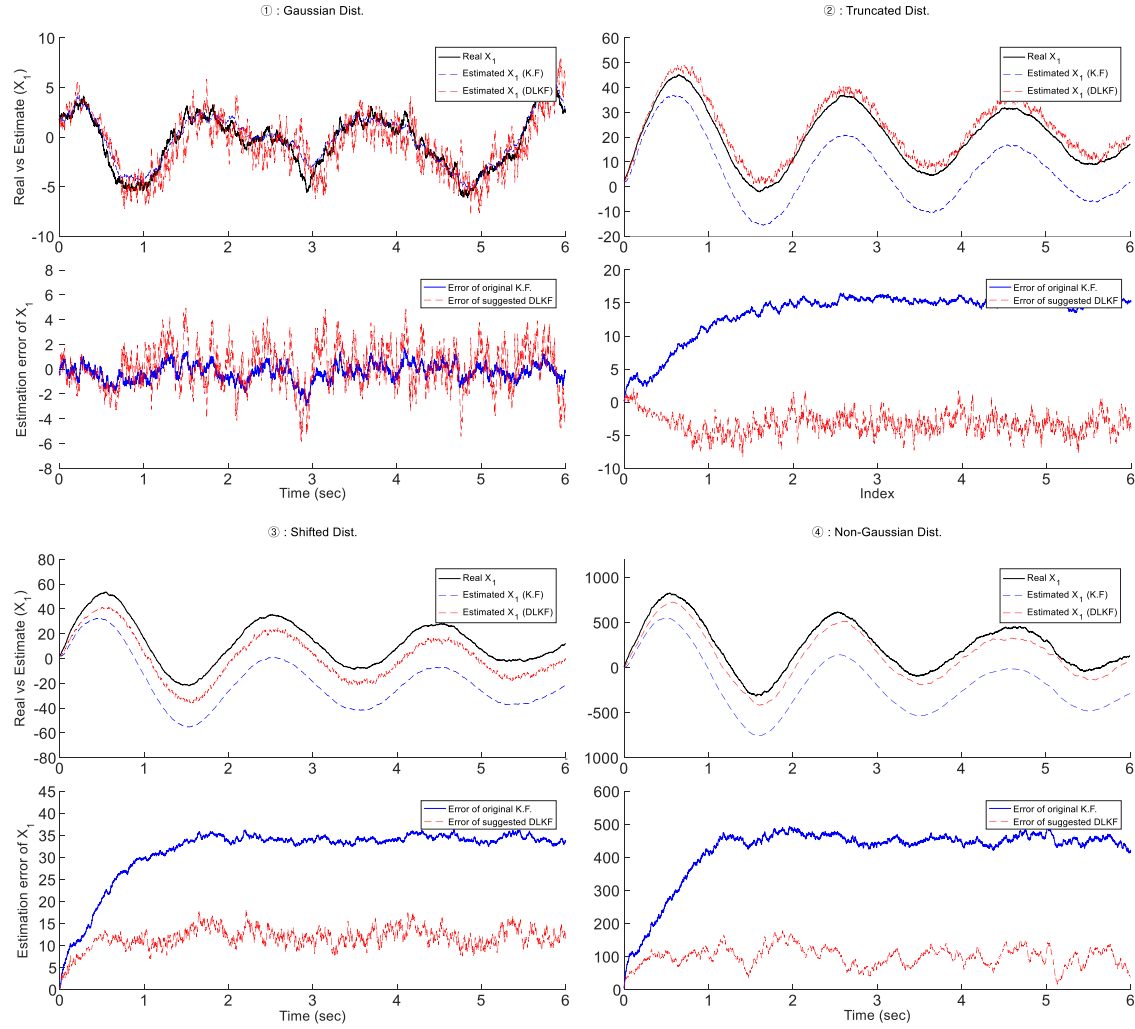


**Fig. 10.** Performance evaluation with regard to four types of disturbances (①Left-top: Gaussian type, ②right-top: Truncated Gaussian type, ③left-bottom: Shifted Gaussian type, ④right-bottom: Non-Gaussian type). In each type, the upper figure shows the estimation result and the lower figure shows the estimation error. Satisfactory estimation can be realized by the existing KFs when the disturbance has a normal-Gaussian distribution. However, the DLKF shows better performance in the case of other types of disturbances.

However, it sometimes shows degraded or divergent results when the system is highly nonlinear or if there are local optima points during the linearization. In the EKF scheme, the estimator suffers from a non-zero-mean/correlated/non-Gaussian modeling error caused by the local linearization process. In contrast, the proposed DLKF scheme is more robust in these cases, because in the DLKF scheme the modeling errors caused by local linearization are estimated by the disturbance estimator and appropriately compensated into the state estimation process. Therefore, it is expected that the proposed DLKF estimator will produce better estimation results than the existing EKF (Extended KF).

A famous gas-phase reaction example was adopted for the nonlinear system state estimation verification test. An ideal gas  $A_g$  is converted into another ideal gas  $B_g$  at some time-varying rate. This system can be summarized as follows. The state is defined as  $x = [P_A P_B]^T$ , where  $P_j$  denotes the partial pressure of gas species  $j$ .

$$x_{k+1} = \begin{bmatrix} \frac{x_{k,1}}{2\bar{k}\Delta t x_{k,1} + 1} \\ x_{k,2} + \frac{\bar{k}\Delta t x_{k,1}^2}{2\bar{k}\Delta t x_{k,1} + 1} \end{bmatrix} + w_k, \quad y_k = [11]x_k + v_k \quad (65)$$

$$\Delta t = 0.1, \quad \bar{k} = 0.16, \quad x_0 = [31]^T,$$

$$Q_K = \text{diag}(0.001^2 \ 0.001^2) \quad R_k = 0.1^2$$

With the system defined in Eq. (65), nonlinear system state estimations are performed using both state estimators (EKF and DLKF). Given that this system is nonlinear, local linearization should be performed at each estimation step. For an exact comparison, both estimators used the same tuning parameters and the same initial conditions:  $\hat{x}_0 = [0.14.5]^T$ ,  $P_0 = \text{diag}(6^2 6^2)$ . Note that the initial estimation guess,  $\hat{x}_0$ , is poor.

The estimation results are shown in Fig. 11. The solid-lines represent the real gas pressure values, the dotted lines represent the estimates provided by the EKF, and the dashed lines represent the estimates obtained from the DLKF. As expected, the DLKF produces better estimates than the EKF. The EKF suffers from the non-zero-mean/correlated/non-Gaussian modeling error caused by linearization. In addition, at the beginning of the estimation process, both EKF and DLKF diverge because of local optima. However, the DLKF is more robust to these factors and can recover from the divergence conditions.

In summary, this section explained the concept, structure, and mathematical implementation of the proposed DLKF. In addition, the DLKF was compared with existing KFs through a few simple examples. The comparisons confirmed that the proposed DLKF estimates the desired state more accurately than the existing KFs,

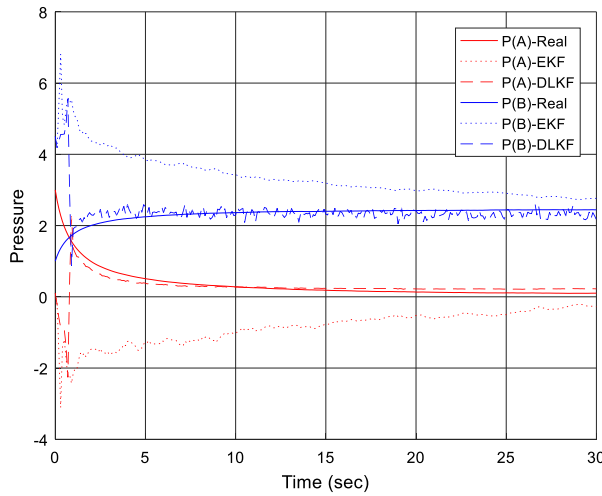


**Fig. 11.** Results of nonlinear system (gas-phase reaction system) state estimation problem. The proposed DLKF shows superior results with respect to the EKF. Both estimators used same tuning parameters and initial conditions.

even in the presence of modeling errors. The next section applies the DLKF to the humanoid robot state estimation problem, which is the main focus of this study.

#### 4. Humanoid state estimation

This section describes the application of the proposed DLKF to the humanoid robot state estimation problem.

##### 4.1. Simulation environment and model

It is extremely important to identify the COM movement and kinematics of humanoid robots under various dynamic situations. In particular, if the current COM information can be obtained accurately when creating a pattern or designing a controller for a biped-walking algorithm, the robots can cope with various environments. Accordingly, the objective of humanoid state estimation in this study is to estimate the COM kinematics (position and velocity).

For the verification test, a simulator was used instead of a real robot. The actual and estimated values should be compared

to evaluate the absolute performance of the estimator. However, it is impossible to measure the real COM (ground-truth COM) accurately owing to various unknown elements of the real robot when it is moving. Therefore, we used a simulator for algorithm verification: the Chorenoid [47] simulator, developed by AIST. The DRC-HUBO was used as a robot model in the simulation. The DRC-HUBO is a humanoid robot developed by KAIST for the DARPA Robotics Challenge (DRC). It has 32 DOF and its height and weight are 170 cm and 80 kg, respectively. In order to input the model into the simulator, the robot was divided into 28 rigid-body parts.

The LIPM shown on the right side of Fig. 12 was used as the time update prediction model in both KF schemes (KF and DLKF). As shown in the figure, the LIPM is an inverted pendulum model characterized by a single point mass and a constant COM height. It has been used in various types of humanoid robots. Although a complex model (i.e. a centroidal model) and full-body dynamics can improve the estimation results, they make the KF implementation significantly difficult and cause the computation time to increase exponentially. In addition, higher-order models make it difficult to tune the estimator parameters. A simple model was deliberately adopted for the purpose of clear performance evaluation of the proposed KF framework. In other words, the purpose of the simple model is to examine the effect of the non-zero and non-Gaussian modeling disturbance. The correlation between the COM and ZMP in the LIPM can be expressed as follows:

$$\begin{aligned}\ddot{x}_{com} &= \frac{g}{h_c}x_{com} - \frac{g}{h_c}P_{zmp,x} \\ \ddot{y}_{com} &= \frac{g}{h_c}y_{com} - \frac{g}{h_c}P_{zmp,y}\end{aligned}\quad (66)$$

where  $P_{zmp,x}$  and  $P_{zmp,y}$  denote the ZMPs along the  $x$ - and  $y$ -axis, respectively, and  $h_c$  denotes the constant height value used in the LIPM. The time update model matrix  $A$  of the KF can be constructed using Eq. (66). As a result of the use of such an extremely simplified model for the time update equation, non-zero/non-Gaussian process noise unavoidably occurs ( $w_k$  is not zero-mean and Gaussian). In these circumstances, it is obvious that the model disturbance ( $w$ ) is correlated with the state ( $x$ ). For the measurement values, two values were employed: the COM position ( $y_1$ ) obtained by the simple forward kinematics and the ZMP value ( $y_2$ ) calculated by the 6-axis F/T (force/torque) sensor located at the ankle of the humanoid robot. Based on the above configuration, the state transition matrix and measurement transition matrix of the KF

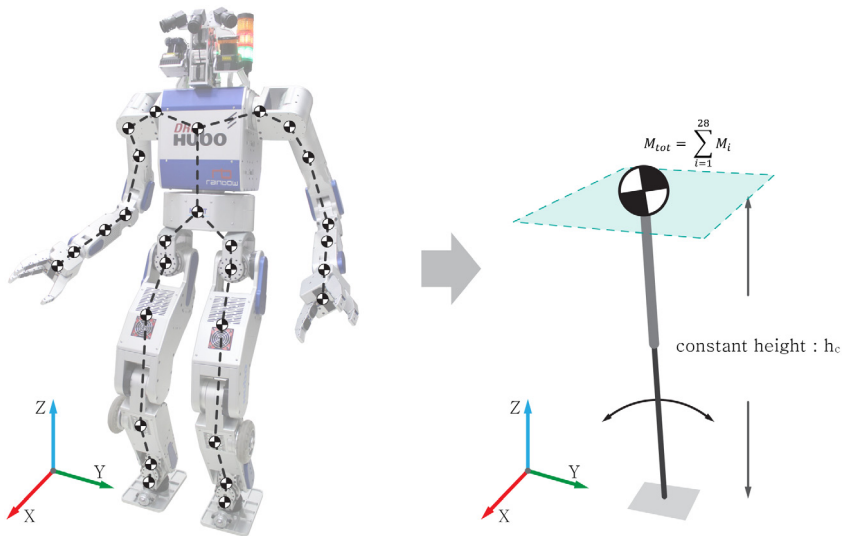


**Fig. 12.** In this simulation, DRC-HUBO was used as a humanoid model. (Left) The model for the simulator consists of 28 rigid-body parts. (Right) As the estimation time update prediction model, a simple LIPM was used. A simple LIPM was chosen in order to focus on the performance evaluation of the proposed DLKF.

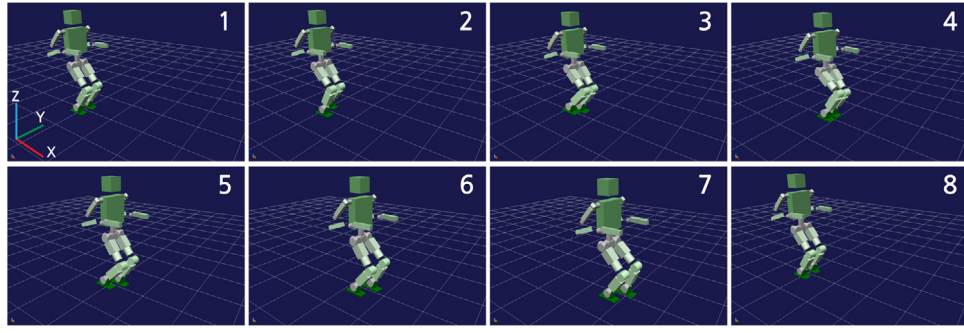


**Fig. 13.** Humanoid robot walking in the Choreonoid simulator. The robot took 10 steps of 10 cm each and COM estimation was performed using the obtained data.

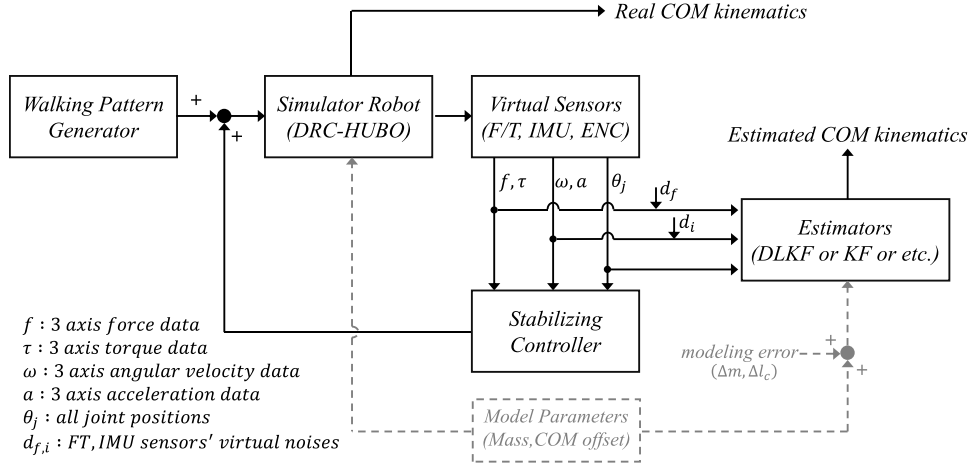


**Fig. 14.** Overall estimation performance evaluation test's schematic diagram. Mass and COM-offset (mass center position of each rigid body link segment) information was intentionally distorted to generate the un-modeled modeling error.

were configured as follows. For the state, the position and velocity of the COM and ZMP were used (state:  $x = [x_{com} \dot{x}_{com} P_{zmp,x}]^T \in R_3$ ).

$$x_{k+1} = A \cdot x_k = \begin{bmatrix} 1 & \Delta t & 0 \\ g/h_c \cdot \Delta t & 1 & -g/h_c \cdot \Delta t \\ 0 & 0 & 1 \end{bmatrix} \cdot x_k \quad (67)$$

$$y_k = \begin{bmatrix} y_{1,k} \\ y_{2,k} \end{bmatrix} = H \cdot x_k = \begin{bmatrix} 1 & 0 & 0 \\ 0 & 0 & 1 \end{bmatrix} \cdot x_k \quad (68)$$

The forward-kinematics-based COM position for the first measurement ( $y_{1,k}$ ) can be obtained easily through  $f_{forward}(\theta_{joint}, R_0)$ , where  $\theta_{joint}$  denotes all the joint angles, and  $R_0 \in R_{3 \times 3}$  denotes the body (pelvis) orientation matrix with respect to the inertial frame  $\Sigma$ . This function can be calculated as follows:

$$y_1 = p_0 + R_0 \frac{\sum_{i=0}^{n_l} M_i ({}^0 p_i + {}^0 R_i p_{G,i})}{M_{tot}} \quad (69)$$

In Eq. (69), the discrete time index  $k$  is omitted for simplicity.  $M_i$  is the mass of link  $i$  (obtained from the CAD model),  $n_l (= 28)$  is the number of links,  $M_{tot} = \sum M_i$  is the total mass of the robot, and  $p_0$  is the position of the link pelvis' COM with respect to the inertial frame  $\Sigma$ . The F/T sensor-based contact estimator and the joint angles are used to calculate the pelvis' position  $p_0$  with respect to  $\Sigma$ . Here, it is assumed that  $R_0$  can guarantee an accurate body orientation, because our target humanoid robot platform DRC-HUBO is equipped with a high-precision fiber optic gyro (FOG) sensor. The variable  ${}^0 p_i$  is the relative position vector of link  $i$  with respect to pelvis frame  $\Sigma_0$  (obtained through the joint angles), and  ${}^i p_{G,i}$  is the relative position of link  $i$ 's COM with respect to individual link frame  $\Sigma_*$  (obtained through the CAD model). At this point, even

though there are CAD modeling errors, the measurement noise of the  $y_1$  ( $v_{1,k}$ ) is assumed to be white Gaussian noise, because the humanoid robot has a symmetric structure. In addition, the noise of the second measurement ( $v_{2,k}$ ) is also assumed to be Gaussian and white, because  $P_{zmp}$  is directly calculated from the raw-F/T sensor data.

The  $y$ -axis COM estimation was performed using the same method.

#### 4.2. Simulation results

In this test, the humanoid robot was made to walk in the simulator and the COM kinematics (position and velocity) were estimated. A pictorial view of the simulation is shown in Fig. 13. The walking step length was 10 cm, and 10 steps were taken. The schematic diagram of the overall estimation performance evaluation system is shown in Fig. 14. As shown, the mass and mass center position of local rigid body frame information was intentionally distorted ( $\Delta m, \Delta l_c = 12\%$  of actual values) in order to generate a modeling error (modeling disturbance) in the estimator. The simulator's sensor data (encoder, IMU, and F/T sensor) was recorded (sampling rate: 200 Hz) during the simulation. In the simulator, virtual Gaussian sensor noise ( $d_f$ ) was added (with zero-mean and  $\pm 5\%$  magnitude covariance) to the F/T sensor. For the encoder data, true joint angle values were used, without noise, because our target humanoid robot platform is controlled based on a high-gain position control. The target estimators used the recorded data in order to estimate the COM kinematics.

The target estimators used the recorded data in order to estimate the COM kinematics. Figs. 15 and 16 show the estimation

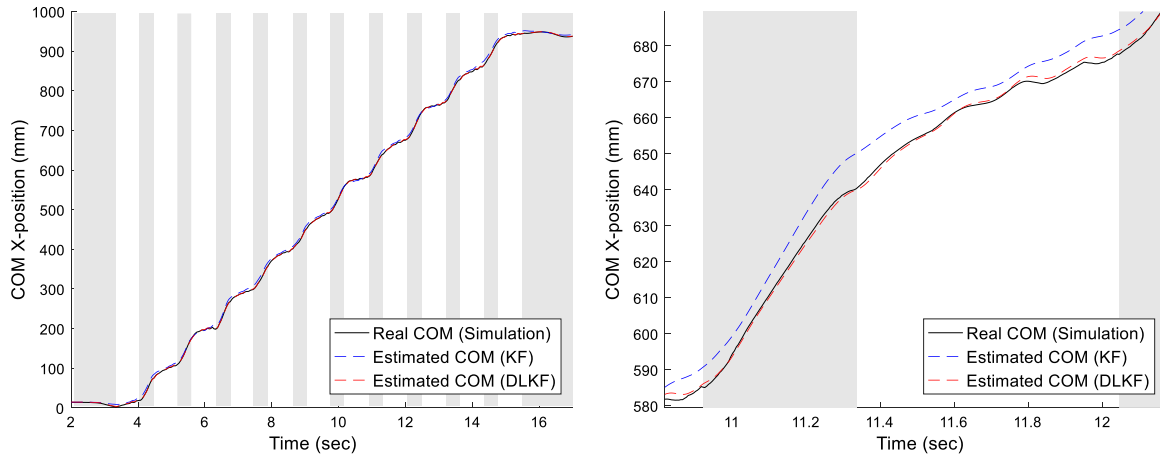


**Fig. 15.** Comparison between true COM value and values estimated using the original KF and proposed estimator (DLKF) along the x-axis. The gray region represents the double support phase (DSP), and the figure on the right is an enlargement of the left figure in the time domain.

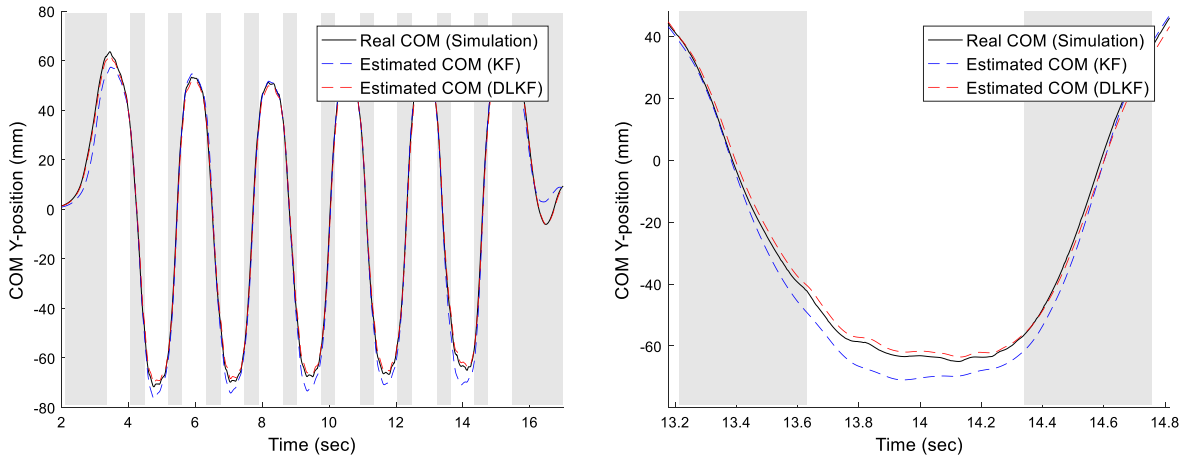


**Fig. 16.** Comparison between true COM value and values estimated using the original KF and proposed estimator (DLKF) along the y-axis. The gray region represents the double support phase (DSP), and the figure on the right is an enlargement of the left figure in the time domain.

results for the COM along the x- and y-axis, respectively. Finally, Fig. 17 shows the errors between the actual COM position and the estimated value along the two axes (the actual COM position could be obtained from the simulator). For fair performance evaluation, the same noise covariance matrix was used as a tuning value for both the conventional KF and the proposed DLKF.

As shown in Figs. 15–17, the test results indicate that the proposed DLKF generates estimates of the COM kinematics that are closer to the true value than those of the conventional KF. This is because the DLKF can estimate the non-Gaussian modeling disturbance generated by the simple LIPM in the disturbance-estimating loop, and effectively provide the estimated result as feedback to the state-estimating loop. On the other hand, the conventional KF is not robust to non-Gaussian noise, as expected. In particular, it suffers from a large error in the double support phase (DSP) section, when both feet are in contact with the ground, i.e., the disturbance increases because of the increased foot contact ( $\approx$  impact). Therefore, the proposed estimator, which consists of two KFs (the state-estimating KF and the disturbance-estimating KF), shows better humanoid state estimation performance than the existing KF when a simple model is used.

In order to verify the performance of the proposed estimator (DLKF) in the humanoid robot state estimation problem, other existing linear estimator frameworks (AKF: augmented KF, CKF: combined KF [46]) and nonlinear estimator frameworks (PF:

particle filter, MHE: moving horizon estimator [48]) were implemented and compared. A moving horizon estimator is a type of full information (FI) estimator that can guarantee a sub-optimal solution within a finite-sized horizon window. Humanoid state estimation with this estimator was developed and discussed in our previous study [48]. The root mean square error, maximum peak error, and relative computational cost associated with the use of each estimator are shown in Table 4. To obtain the results in this table, 500 particles were used for the PF, and a horizon size of 30 was used for the MHE. These results show that the proposed DLKF produces better estimates in the humanoid state estimation problem than the existing linear or nonlinear estimators.

However, if there is additional nonlinear system information such as inequality constraints (i.e., ZMP boundary conditions), the PF or MHE can be alternative methods for state estimation. So far, our proposed DLKF cannot handle such inequality constraints directly. This issue will be addressed in future work.

In order to verify the feasibility of the proposed estimator (DLKF), the algorithm was implemented on a real DRC-HUBO robot platform. The results obtained for COM estimation using the proposed DLKF-based estimator with the real humanoid robot are shown in Fig. 18. In the experiment, the robot executed eight 15-cm forward steps, for a total distance of 1.2 m. In the real environment, it is impossible to accurately acquire the actual COM position (ground-truth value) because of the various unknown

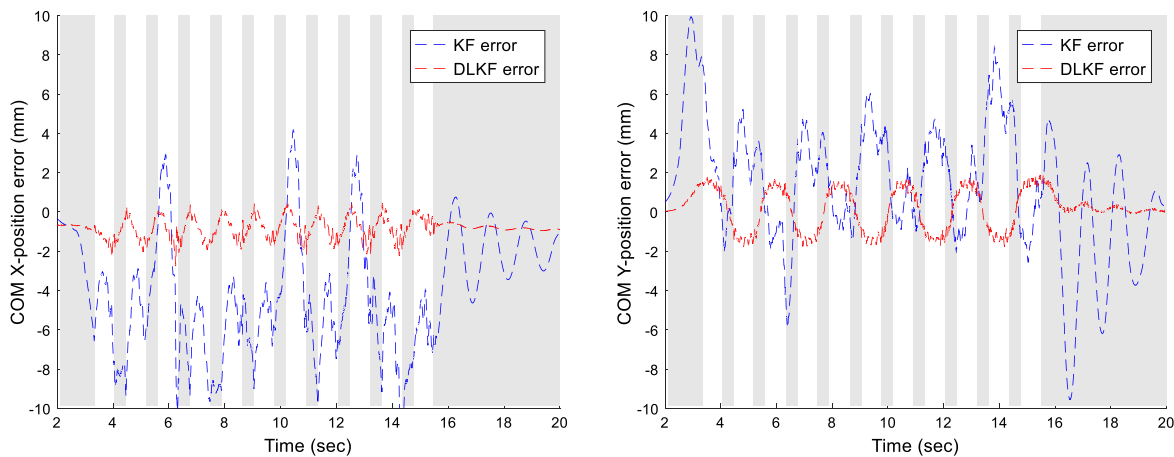


**Fig. 17.** (Left) Estimation error of the two KFs along the x-axis (Right) Estimation error of the two KFs along the y-axis. In both the directions, the proposed DLKF estimated the COM kinematics more accurately than the original KF. The gray region represents the double support phase (DSP) in which both feet are on the ground while walking.

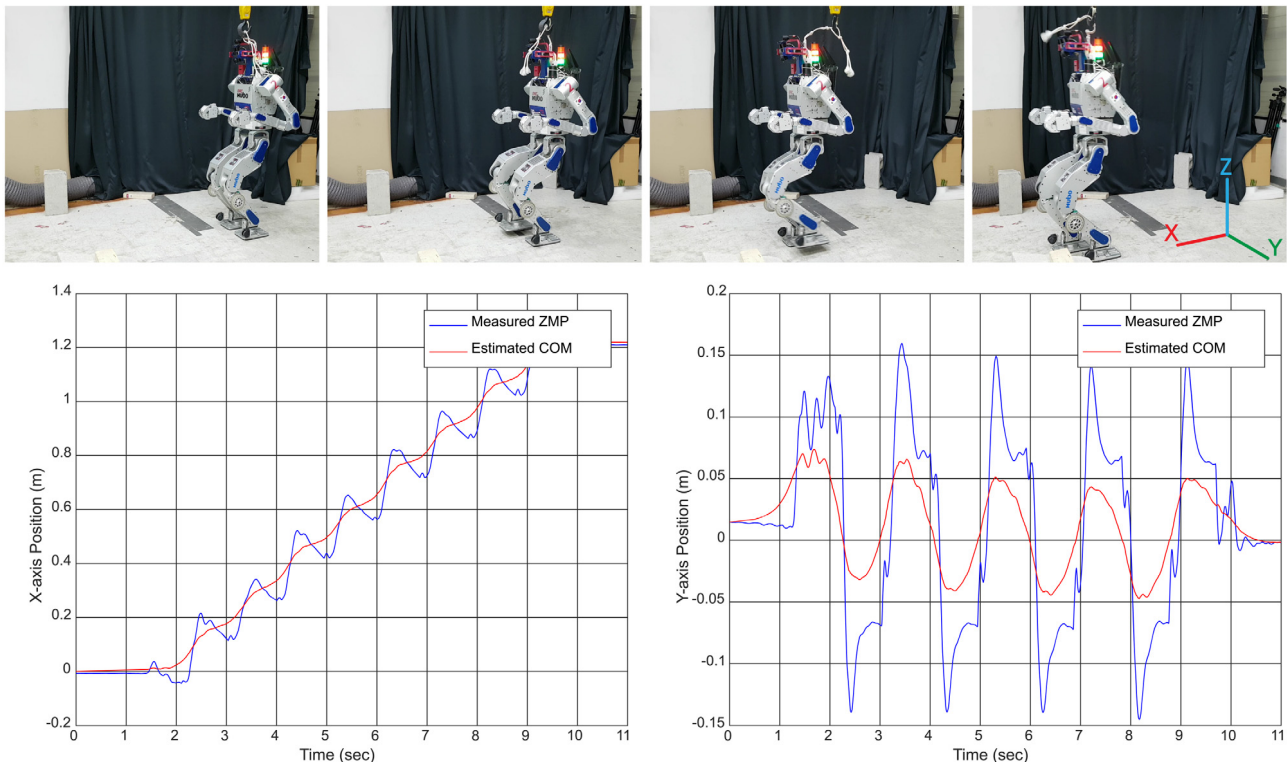


**Fig. 18.** COM position (x and y axes) estimation result using the proposed DLKF-based estimator with the real humanoid robot DRC-HUBO. The robot took eight steps, each 15 cm in length, and COM estimation was performed in real-time. ZMP is measured by F/T sensors on the foot. (Left: x-axis, Right: y-axis).

**Table 4**  
Comparison of six state estimators in terms of computation time and accuracy (unit: mm).

	KF	AKF	CKF	PF	MHE	DLKF
X axis	RMS error	4.528	1.666	0.928	1.455	1.899
	Peak error	12.250	4.984	3.395	6.069	5.391
Y axis	RMS error	3.287	1.024	1.332	1.728	1.097
	Peak error	9.934	3.252	3.072	5.474	3.529
Relative computation cost	1	1.8	5.8	221	140	8.5

aspects of the real robot's behavior when it is moving. Therefore, the actual COM position is not presented in the figure showing the estimation results. However, the results show that the proposed

DLKF-based state estimator did produce smooth and continuous estimated values, and did so in real-time.

## 5. Conclusion

This study proposed a novel estimation framework to overcome the shortcomings of the conventional Kalman filter-based approaches, and applied the proposed framework to a humanoid state estimation problem. The conventional Kalman filter can guarantee optimal estimation results if the modeling errors are uncorrelated and follow a zero-mean Gaussian distribution. When those errors are not Gaussian distributed, the KF is still the best linear estimator; however, it cannot cope with correlated or non-zero-mean modeling errors. In such a case its optimality is lost.

The proposed KF framework, which is robust to modeling errors, overcomes the above-mentioned problem. The proposed estimator is a dual-loop Kalman filter (DLKF), which consists of a KF for state estimation, a disturbance detector to measure disturbances, and a KF for disturbance estimation, based on the measured disturbances. The estimated disturbance is fed back to the state estimator, thereby improving the model prediction accuracy. During this process, the correlation between the state vector and the disturbance vector is carefully considered. Consequently, this disturbance compensation acts like a residual-error-integration compensator. Therefore, the proposed DLKF yields more accurate and robust humanoid state estimation results than the original Kalman filter, even when using a simple model with large modeling errors.

The superiority of the DLKF was verified through frequency analysis and humanoid robot simulation tests. In particular, the proposed estimator shows a highly improved performance in dynamic situations where the modeling noise increases. In addition, the proposed estimator was compared with other existing linear and nonlinear estimation frameworks—such as augmented KF (AKF), combined KF (CKF), moving horizon estimator (MHE) and particle filter (PF), in terms of robustness, accuracy, and efficiency. Unlike other robust KFs that require the solution of Riccati equations and require uncertainty-bounding conditions, the proposed estimator is based on a simple structure. Therefore, it can facilitate a recursive online implementation. Finally, the feasibility of DLKF was verified by implementing it on a real humanoid robot platform, where it produced smooth and continuous COM kinematics estimation results in real-time.

In the present study, a simple LIPM model was used, so that the focus could be placed on the evaluation of the proposed estimator's performance. However, the applicability of this model is extremely limited. It is valid only when the robot walks on flat terrain and when at least one foot is in contact with the ground. In addition, with the suggested DLKF framework, it is difficult to cope with various inequality constraints. Therefore, in future work, a more systematic and accurate estimator structure/model based on the proposed DLKF will be designed, to better cope with the various humanoid motions.

## Acknowledgment

This research did not receive any specific grant from funding agencies in the public, commercial, or not-for-profit sectors.

## References

- [1] I.W. Park, J.Y. Kim, J. Lee, J.H. Oh, Mechanical design of humanoid robot platform KHR-3 (KAIST humanoid robot - 3: HUBO), in: Proc. 2005 5th IEEE-RAS Int. Conf. Humanoid Robot., vol. 2005, 2005, pp. 321–326. <http://dx.doi.org/10.1109/ICHR.2005.1573587>.
- [2] M. Johnson, B. Shrewsbury, S. Bertrand, T. Wu, D. Duran, M. Floyd, P. Abeles, D. Stephen, N. Mertins, A. Lesman, J. Carff, W. Rifenburgh, P. Kaveti, W. Straatman, J. Smith, M. Griffioen, B. Layton, T. De Boer, Team IHMC 's lessons learned from the DARPA robotics challenge trials, *J. F. Robot.* 32 (2015) 192–208. <http://dx.doi.org/10.1002/rob>.
- [3] M. Hirose, K. Ogawa, Honda humanoid robots development, *Philos. Trans. R. Soc. A Math. Phys. Eng. Sci.* 365 (2007) 11–19. <http://dx.doi.org/10.1098/rsta.2006.1917>.
- [4] K. Kaneko, K. Harada, F. Kanehiro, G. Miyamori, K. Akachi, Humanoid robot HRP-3, in: 2008 IEEE/RSJ Int. Conf. Intell. Robot. Syst., IROS, 2008, pp. 2471–2478. <http://dx.doi.org/10.1109/IROS.2008.4650604>.
- [5] J. Urata, Y. Nakanishi, K. Okada, M. Inaba, Design of high torque and high speed leg module for high power humanoid, in: IEEE/RSJ 2010 Int. Conf. Intell. Robot. Syst., IROS 2010 – Conf. Proc., 2010, pp. 4497–4502. <http://dx.doi.org/10.1109/IROS.2010.5649683>.
- [6] S. Park, Y. Han, H. Hahn, Kalman filter based zmp estimation scheme for balance control of a biped robot, in: The 4th International Conference on Ubiquitous Robots and Ambient Intelligence URAI, 2007.
- [7] S. Kwon, Y. Oh, Estimation of the center of mass of humanoid robot, ICCAS 2007 - Int. Conf. Control. Autom. Syst., 2007, pp. 2705–2709. <http://dx.doi.org/10.1109/ICCAS.2007.4406826>.
- [8] Xinjilefu, C.G. Atkeson, State estimation of a walking humanoid robot, *IEEE Int. Conf. Intell. Robot. Syst.* (2012) 3693–3699. <http://dx.doi.org/10.1109/IROS.2012.6386070>.
- [9] K. Masuya, T. Sugihara, COM motion estimation of a humanoid robot based on a fusion of dynamics and kinematics information, in: IEEE Int. Conf. Intell. Robot. Syst., vol. 2015, December, 2015, pp. 3975–3980. <http://dx.doi.org/10.1109/IROS.2015.7353937>.
- [10] X. Xinjilefu, S. Feng, W. Huang, C.G. Atkeson, Decoupled state estimation for humanoids using full-body dynamics, in: Proc. - IEEE Int. Conf. Robot. Autom., 2014, pp. 195–201. <http://dx.doi.org/10.1109/ICRA.2014.6906609>.
- [11] M.F. Fallon, M. Antone, N. Roy, S. Teller, Drift-free humanoid state estimation fusing kinematic, inertial and LIDAR sensing, in: IEEE-RAS Int. Conf. Humanoid Robot., vol. 2015–February, 2015, pp. 112–119. <http://dx.doi.org/10.1109/HUMANOIDS.2014.7041346>.
- [12] S. Kuindersma, R. Deits, M. Fallon, A. Valenzuela, H. Dai, F. Permenter, T. Koolen, P. Marion, R. Tedrake, Optimization-based locomotion planning, estimation, and control design for the atlas humanoid robot, *Auton. Robots.* 40 (2016) 429–455. <http://dx.doi.org/10.1007/s10514-015-9479-3>.
- [13] M. Bloesch, M. Hutter, M. Hoepflinger, S. Leutenegger, C. Gehring, C. David Remy, R. Siegwart, State estimation for legged robots - consistent fusion of leg kinematics and IMU, *Robot. Sci. Syst. VIII* (2012). <http://dx.doi.org/10.15607/RSS.2012.VIII.003>.
- [14] N. Rotella, M. Bloesch, L. Righetti, S. Schaal, State estimation for a humanoid robot, in: IEEE/RSJ Int. Conf. Intell. Robot. Syst., 2014, pp. 952–958. <http://dx.doi.org/10.1109/RSJ.2014.6942674>.
- [15] Pei-Chun Lin, H. Komsuoglu, D.E. Koditschek, Sensor data fusion for body state estimation in a hexapod robot with dynamical gaits, *IEEE Trans. Robot.* 22 (2006) 932–943. <http://dx.doi.org/10.1109/TRO.2006.878954>.
- [16] M. Benallegue, F. Lamiriaux, Humanoid flexibility deformation can be efficiently estimated using only inertial measurement units and contact information, in: IEEE-RAS Int. Conf. Humanoid Robot., IEEE, 2014, pp. 246–251. <http://dx.doi.org/10.1109/HUMANOIDS.2014.7041367>.
- [17] A. Misud, M. Benallegue, F. Lamiriaux, Estimation of contact forces and floating base kinematics of a humanoid robot using only inertial measurement units, in: 2015 IEEE/RSJ Int. Conf. Intell. Robot. Syst., 2015, pp. 3374–3379. <http://dx.doi.org/10.1109/RSJ.2015.7353847>.
- [18] X. Xinjilefu, S. Feng, C.G. Atkeson, A distributed MEMS gyro network for joint velocity estimation, in: IEEE Int. Conf. Robot. Autom., IEEE, 2016, pp. 1879–1884. <http://dx.doi.org/10.1109/ICRA.2016.7487334>.
- [19] J. Eljaik, N. Kuppuswamy, F. Nori, Multimodal sensor fusion for foot state estimation in bipedal robots using the extended Kalman filter, in: 2015 IEEE/RSJ Int. Conf. Intell. Robot. Syst., 2015, pp. 2698–2704. <http://dx.doi.org/10.1109/RSJ.2015.7353746>.
- [20] G. Welch, G. Bishop, *An Introduction to the Kalman Filter*, 1995.
- [21] A.P. Anrews, *Kalman Filtering: Theory and Practice using MATLAB*, John Wiley & Sons, ISBN: 9780471392545, 2001.
- [22] D. Simon, *Optimal State Estimation: Kalman, H Infinity, and Nonlinear Approaches*, John Wiley & Sons, ISBN: 9780471708582, 2006.
- [23] S. Kajita, F. Kanehiro, K. Kaneko, K. Yokoi, H. Hirukawa, The 3D linear inverted pendulum mode: a simple modeling for a biped walking pattern generation, in: Proc. 2001 IEEE/RSJ Int. Conf. Intell. Robot. Syst. Expand. Soc. Role Robot. Next Millenn. (Cat. No.01CH37180), vol. 1, 2001, pp. 239–246. <http://dx.doi.org/10.1109/RSJ.2001.973365>.
- [24] S. Kajita, F. Kanehiro, K. Kaneko, K. Fujiwara, K. Yokoi, H. Hirukawa, A realtime pattern generator for biped walking, in: Proc. 2002 IEEE Int. Conf. Robot. Autom. (Cat. No.02CH37292), vol. 1, 2002, pp. 31–37. <http://dx.doi.org/10.1109/ROBOT.2002.1013335>.
- [25] X. Xinjilefu, S. Feng, C.G. Atkeson, Dynamic state estimation using quadratic programming, in: 2014 IEEE/RSJ Int. Conf. Intell. Robot. Syst., 2014, pp. 989–994. <http://dx.doi.org/10.1109/RSJ.2014.6942679>.
- [26] K. Masuya, T. Sugihara, Dead reckoning for biped robots that suffers less from foot contact condition based on anchoring pivot estimation, *Adv. Robot.* 29 (2015) 785–799. <http://dx.doi.org/10.1080/01691864.2015.1011694>.
- [27] L. Pongsak, O. Masafumi, Y. Nakamura, Optimal filtering for humanoid robot state estimators, in: Proc. SICE Syst. Integr. Div. Annu. Conf., 2002, pp. 5–6.
- [28] K. Kaneko, F. Kanehiro, S. Kajita, M. Morisawa, K. Fujiwara, K. Harada, H. Hirukawa, Slip observer for walking on a low friction floor, 2005 IEEE/RSJ Int. Conf. Intell. Robot. Syst. IROS, 2005, pp. 1457–1463. <http://dx.doi.org/10.1109/RSJ.2005.1545184>.
- [29] B.J. Stephens, State estimation for force-controlled humanoid balance using simple models in the presence of modeling error, in: Proc. - IEEE Int. Conf. Robot. Autom., 2011, pp. 3994–3999. <http://dx.doi.org/10.1109/ICRA.2011.5980358>.
- [30] X. Xinjilefu, S. Feng, C.G. Atkeson, Center of mass estimator for humanoids and its application in modelling error compensation, fall detection and prevention, in: IEEE-RAS Int. Conf. Humanoid Robot., vol. 2015–December, 2015, pp. 67–73. <http://dx.doi.org/10.1109/HUMANOIDS.2015.7363533>.

- [31] R. Wittmann, A.-C. Hildebrandt, D. Wahrmann, D. Rixen, T. Buschmann, State estimation for biped robots using multibody dynamics, in: IEEE/RSJ Int. Conf. Intell. Robot. Syst., IEEE, 2015, pp. 2166–2172. <http://dx.doi.org/10.1109/IROS.2015.7353667>.
- [32] S. Piperakis, P. Trahanias, Non-Linear ZMP based state estimation for humanoid robot locomotion, 2016 IEEE-RAS Int. Conf. Humanoid Robot., Humanoids 2016, 2016. <http://dx.doi.org/10.1109/HUMANOIDS.2016.7803278>.
- [33] Lihua Xie, Yeng Chai Soh, C.E. de Souza, Robust Kalman filtering for uncertain discrete-time systems, IEEE Trans. Automat. Control 39 (1994) 1310–1314. <http://dx.doi.org/10.1109/9.293203>.
- [34] G.A. Terejanu, Extended Kalman Filter Tutorial, University at Buffalo, 2008.
- [35] S.J. Julier, J.K. Uhlmann, A new extension of the Kalman filter to nonlinear systems, in: 11th Symp. Aerospace/Defense Sens. (AeroSense), Simulations Control, vol. 3068, 1997, pp. 182–193. <http://dx.doi.org/10.1117/12.280797>.
- [36] G. Evensen, The ensemble Kalman filter: Theoretical formulation and practical implementation, Ocean Dyn. 53 (2003) 343–367. <http://dx.doi.org/10.1007/s10236-003-0036-9>.
- [37] D.W. Gu, F.W. Poon, A robust state observer scheme, IEEE Trans. Automat. Control 46 (2001) 1958–1963. <http://dx.doi.org/10.1109/9.975500>.
- [38] Fuwen Yang, Zidong Wang, Y.S. Hung, Robust Kalman filtering for discrete time-varying uncertain systems with multiplicative noises, IEEE Trans. Automat. Control 47 (2002) 1179–1183. <http://dx.doi.org/10.1109/TAC.2002.800668>.
- [39] W.H. Chen, D.J. Ballance, P.J. Gawthrop, J. O'Reilly, A nonlinear disturbance observer for robotic manipulators, IEEE Trans. Ind. Electron. 47 (2000) 932–938. <http://dx.doi.org/10.1109/41.857974>.
- [40] K. Ohnishi, M. Shibata, T. Murakami, Motion control for advanced mechatronics, IEEE/ASME Trans. Mechatronics 1 (1996) 56–67. <http://dx.doi.org/10.1109/3516.491410>.
- [41] T. Umeno, Y. Hori, Robust speed control of DC servomotors using modern two degrees-of-freedom controller design, IEEE Trans. Ind. Electron. 38 (1991) 363–368. <http://dx.doi.org/10.1109/41.97556>.
- [42] J.-H. Kim, J.-H. Oh, Robust state estimator of stochastic linear systems with unknown disturbances, IEE Proc. D 147 (2000) 224–228. <http://dx.doi.org/10.1049/ip-cta:20000174>.
- [43] S.J. Kwon, S.D. Park, S.M. Lee, A perturbation observer based robust estimation technique for structural monitoring and control, Solid State Phenom. 120 (2007) 241–246. <http://dx.doi.org/10.4028/www.scientific.net/SSP.120.241>.
- [44] S. Kwon, W.K. Chung, Combined synthesis of state estimator and perturbation observer, J. Dyn. Syst. Meas. Control 125 (2003) 19. <http://dx.doi.org/10.1115/1.1540112>.
- [45] S.J. Kwon, W.K. Chung, A discrete-time design and analysis of perturbation observer for motion control applications, IEEE Trans. Control Syst. Technol. 11 (2003) 399–407. <http://dx.doi.org/10.1109/TCST.2003.810398>.
- [46] S.J. Kwon, Robust Kalman filtering with perturbation estimation process for uncertain systems, IEE Proc. D 153 (2006) 600–606. <http://dx.doi.org/10.1049/ip-cta:20050452>.
- [47] Choreonoid simulator official site: <http://choreonoid.org/en/>.
- [48] H. Bae, J.-H. Oh, Humanoid state estimation using a moving horizon estimator, Adv. Robot. 1864 (2017) 1–11. <http://dx.doi.org/10.1080/01691864.2017.1326317>.



**Hyo-in Bae** received his B.S. degree in Mechanical Engineering from Korea Advanced Institute of Science and Technology (KAIST), Daejeon, South Korea, and M.S. in Mechanical Engineering from KAIST, in 2012 and 2014, respectively. Since 2014, he is currently pursuing the Ph.D. degree in Mechanical engineering at the KAIST and working on the project of development for humanoid robots: HUBO2 and DRC-HUBO. His research interests include state estimation for multi degree of freedom system, disturbance estimation, humanoid robot design, and sensor fusion algorithm.



**Jun-Ho Oh** received his B.S. and M.S. degrees in Mechanical Engineering from Yonsei University, Seoul, South Korea, and has Ph.D. degree in Mechanical Engineering from University of California, Berkeley, in 1977, 1979, and 1985 respectively. He was a Researcher with the Korea Atomic Energy Research Institute, from 1979 to 1981. Since 1985, he has been with the Department of Mechanical Engineering, KAIST, where he is currently a significant professor and a director of Humanoid Robot Research Center. And he has been a vice president of KAIST since 2013. He was a Visiting Research Scientist in the University of Texas Austin, from 1996 to 1997. His research interests include humanoid robots, adaptive control, intelligent control, nonlinear control, biomechanics, sensors, actuators, and application of micro-processor. Dr. Oh is a member of the IEEE, KSME, KSPE and ICASE.